eLIFE
elifesciences.org

RESEARCH ARTICLE

Figures and figure supplements

The cell proliferation antigen Ki-67 organises heterochromatin

Michal Sobecki *et al*

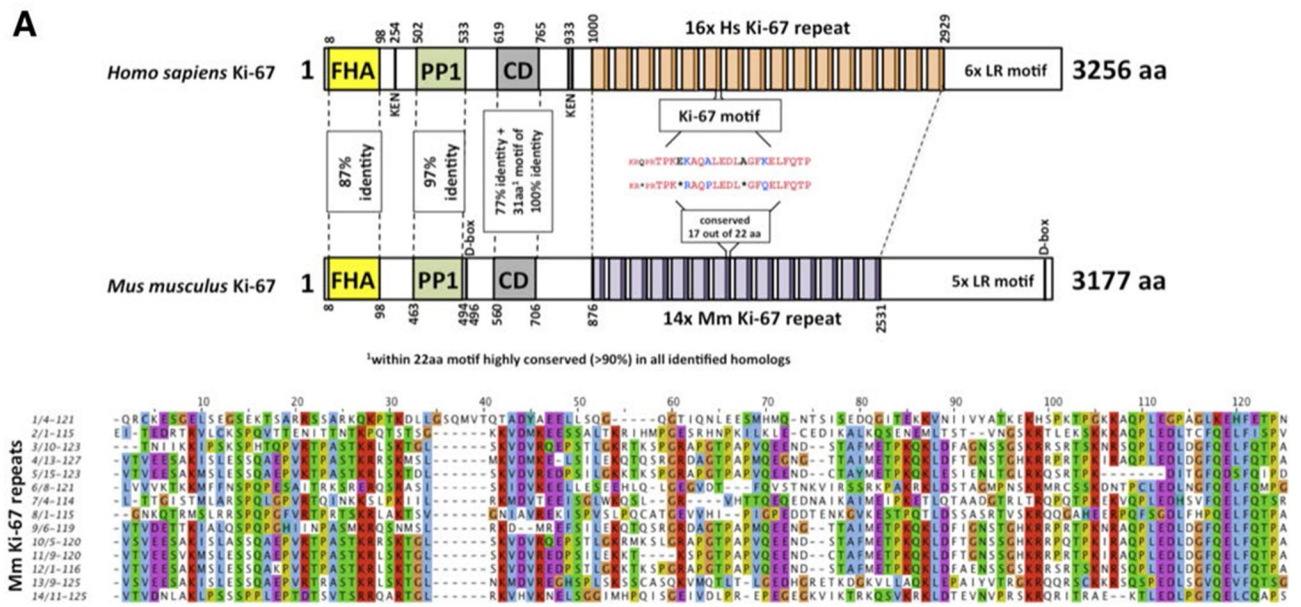

B

Position	Peptide	Score	Cutoff	Type
Human Ki-67 isoform 1				
254-256	ELDVKSQKENVLQYCRK	17.59	8.28	KEN
933-935	ERPFETYKENIELKEND	16.09	8.28	KEN
939-941	YKENIELKENDEKMKAM	18.59	8.28	KEN
Human Ki-67 isoform 2				
573-575	ERPFETYKENIELKEND	16.09	8.28	KEN
579-581	YKENIELKENDEKMKAM	18.59	8.28	KEN
Mouse Ki-67				
496-499	RGETPTKRKSLGTHSPAV	5.88	5.16	D
3139-3142	CLRSRKTRVALDESPKPR	5.69	5.16	D

Figure 1. Comparison of human and mouse Ki-67 structural elements. (**A**) Top: cartoon of human (long form) and mouse Ki-67 protein highlighting conserved elements and functional motifs. Domains are indicated by boxes (FHA, forkhead-associated domain; PP1, PP1-binding domain; CD, conserved domain; D-box: APC/C targeting destruction box motifs; KEN: APC/C-Cdh1 targeting KEN box motifs). Highly conserved regions are indicated by dotted line with percent of identical amino acids. Bottom: alignment of mouse Ki-67 repeats. (**B**) APC/C targeting motifs identified in human (both isoforms) and mouse Ki-67.

DOI: 10.7554/eLife.13722.003

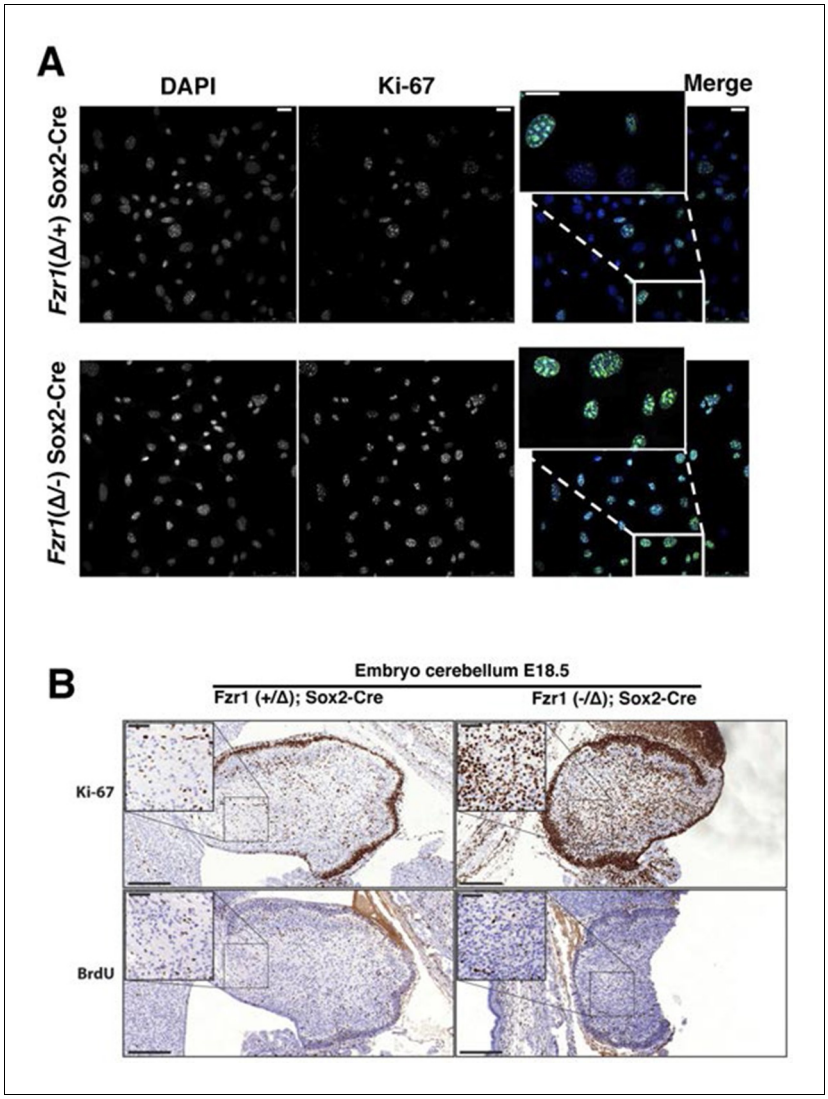

Figure 2. Maintenance of Ki-67 expression in quiescent cells in vivo by Cdh1 mutation. (**A**) Immunofluorescence analysis of Ki-67 in MEF cells isolated from embryo (E13.5) of *Fzr1*(+/Δ);*Sox2*-Cre and Fzr1(-/Δ);*Sox2*-Cre mice. Scale bar, 25 μm. (**B**) IHC staining of Ki-67 and BrdU in sagittal sections of embryo cerebellum (E18.5) of *Fzr1* (+/Δ); *Sox2*-Cre and *Fzr1* (-/Δ);*Sox2*-Cre mice. Bars, 200 μm. Bars in zoom, 50 μm.

DOI: 10.7554/eLife.13722.004

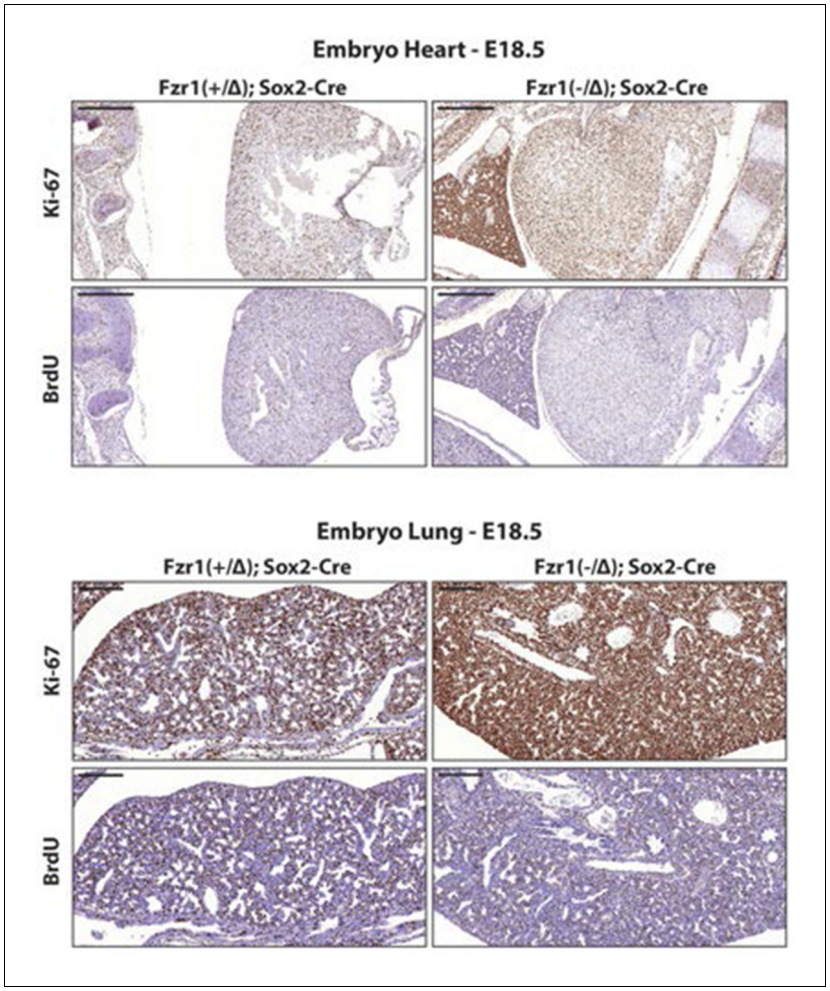

Figure 2—figure supplement 1. Ki-67 expression is restricted to proliferating cells by APC/C-Cdh1. Top, IHC staining of Ki-67 and BrdU in sagittal section of embryo heart (E18.5) of *Fzr1*$^{(+/\Delta)}$;*Sox2-Cre* and *Fzr1*$^{(-/\Delta)}$;*Sox2-Cre* mice. Scale bar, 500 μm. Bottom, IHC staining of Ki-67 and BrdU in sagittal section of embryo lung (E18.5) of *Fzr1*$^{(+/\Delta)}$;*Sox2-Cre* and *Fzr1*$^{(-/\Delta)}$;*Sox2-Cre* mice. Scale bar, 200 μm.

DOI: 10.7554/eLife.13722.005

A

Mice	Sequence	Mutation	Feature
WT	TCCGCCCTGGTCCGCAGTCCCGACGGCCGGGCGGACCATGGCGTCCTCGGCTCACCTGGTCACCATCAAG		
M1	TCCGCCCTGGTCCGCAGTCCCGACGGCCGGGCGGACCATGGC..CCTCGGCTCACCTGGTCACCATCAAG	2nt del	frameshift
M2	TCCGCCCTGGTCCGCAGTCCCGACGGCCG.....CTCACCTGGTCACCATCAAG	21nt del	deletion of 1st ATG
M3	TCCGCCCTGGTCCGCAGTCCCGACGGCCGGGCGGACCATG...TCCTCGGCTCACCTGGTCACCATCAAG	3nt del	
M4	TCCGCCCTGGTCCGCAGTCCCGACGGC.....TCACCTGGTCACCATCAAG	24nt del	deletion of 1st ATG
M5	TCCGCCCTGGTCCGCAGTCCCGACGGCCGGGCGGACCATGG.GTCCTCGGCTCACCTGGTCACCATCAAG	1nt del	frameshift
M6	TCCGCCCTGGTCCGCAGTCCCGACGGCCGGGCGGACCATGGC.TCCTCGGCTCACCTGGTCACCATCAAG	1nt del	frameshift

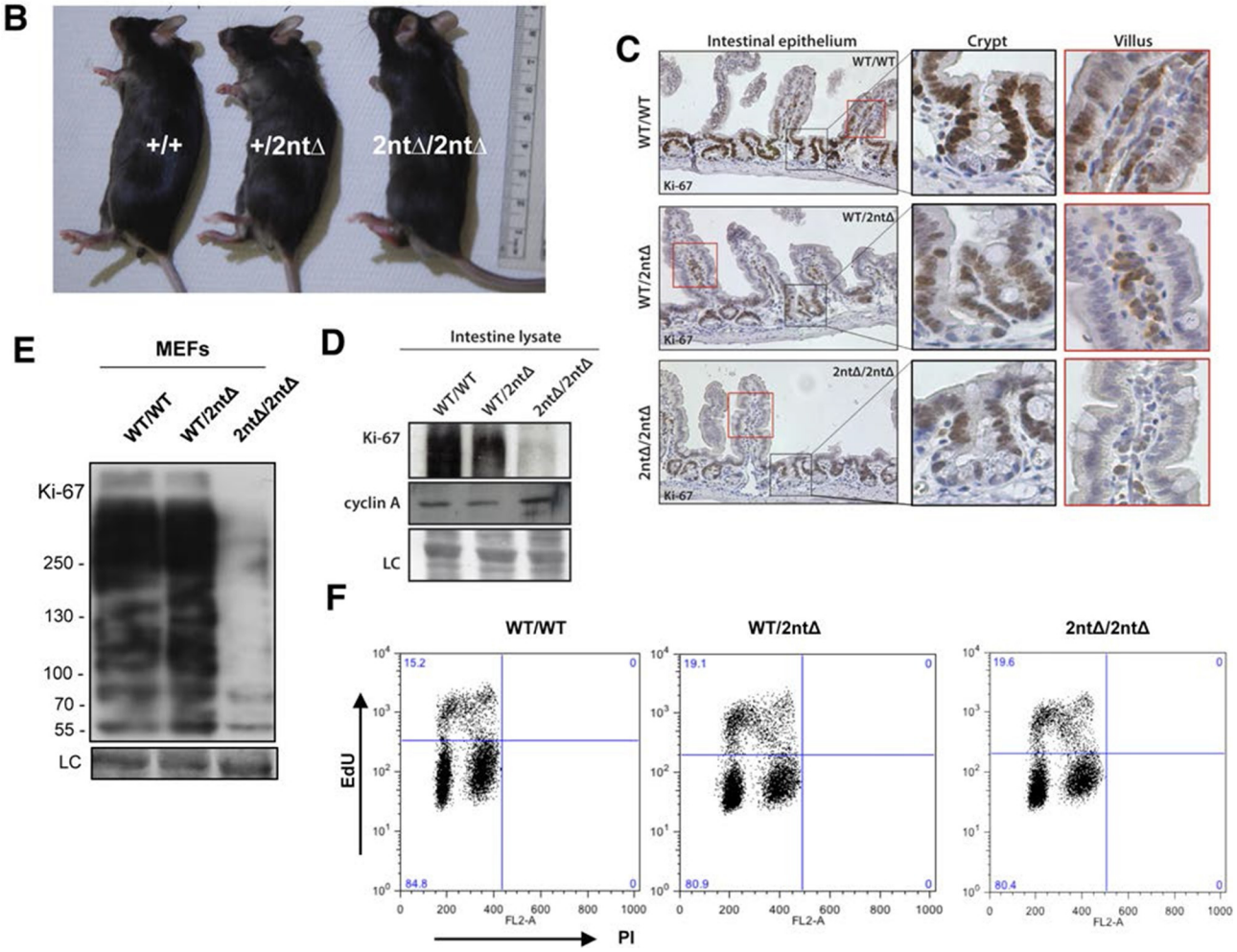

Figure 3. Mouse development with a mutated Ki-67 gene. (**A**) Table describing Ki-67 mutant mouse lines resulting from germline transmission of mutations generated by cytoplasmic injection of TALEN-encoding mRNA into zygotes. (**B**) Macroscopic appearance of littermate female mice at 10 weeks of age. Genotypes are specified. (**C**) IHC staining of Ki-67 in sagittal section of intestine from *Mki67*$^{WT/WT}$, *Mki67*$^{WT/2ntΔ}$ and Mki67$^{2ntΔ/2ntΔ}$ mice. (**D**) Western blots of Ki-67 and cyclin A expression from intestine isolated from *Mki67*$^{WT/WT}$, *Mki67*$^{WT/2ntΔ}$ and *Mki67*$^{2ntΔ/2ntΔ}$ mice. LC, loading control. (**E**) Western blot of Ki-67 in MEFs from WT, *Mki67*$^{WT/2ntΔ}$ and *Mki67*$^{2ntΔ/2ntΔ}$ mice. LC, loading control. (**F**) Flow cytometry profiles in WT, *Mki67*$^{WT/2ntΔ}$ and *Mki67*$^{2ntΔ/2ntΔ}$ MEFs showing EdU incorporation upon a 1 hr pulse and DNA content.

DOI: 10.7554/eLife.13722.006

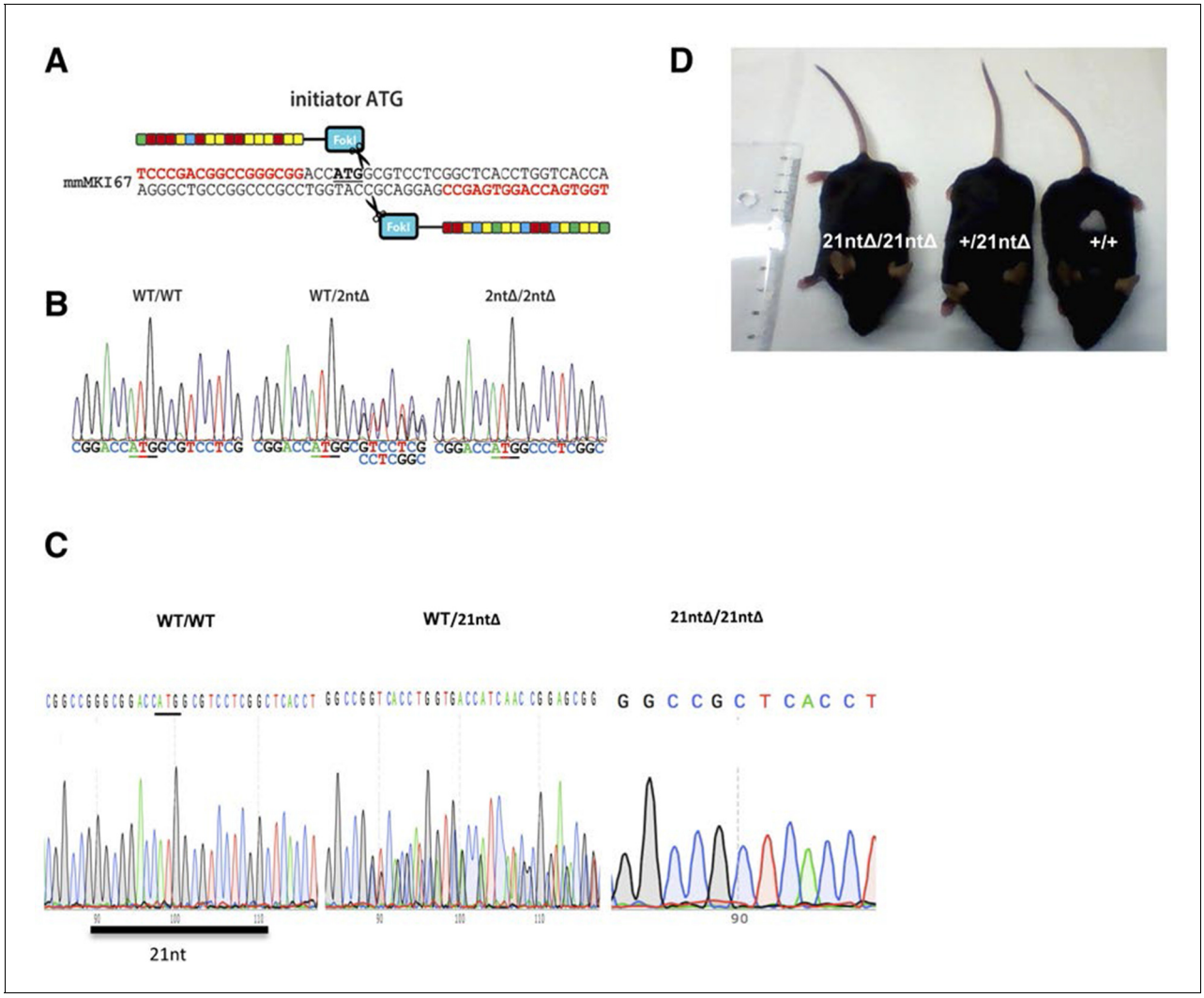

Figure 3—figure supplement 1. Ki-67 mutant mice develop normally. (**A**) Pair of TALE-nucleases designed to target the initiator ATG of mouse *Mki67* gene. (**B**) Sequencing traces of initiator ATG (underlined) of *Mki67* gene in WT *Mki67*$^{+/+}$ (WT/WT), heterozygous *Mki67*$^{+/2ntΔ}$(WT/2ntΔ) and homozygous *Mki67*$^{2ntΔ/2ntΔ}$(2ntΔ/2ntΔ) mice. (**C**) Sequencing traces of initiator ATG (underlined) of *Mki67* gene in WT *Mki67*$^{+/+}$ (WT/WT), heterozygous *Mki67*$^{+/21ntΔ}$(WT/21ntΔ) and homozygous *Mki67*$^{21ntΔ/21ntΔ}$(21ntΔ/21ntΔ) mice. (**D**) WT *Mki67*$^{+/+}$ (+/+), heterozygous *Mki67*$^{+/21ntΔ}$(+/21ntΔ) and homozygous *Mki67*$^{21ntΔ/21ntΔ}$(21ntΔ/21ntΔ) mice.

DOI: 10.7554/eLife.13722.007

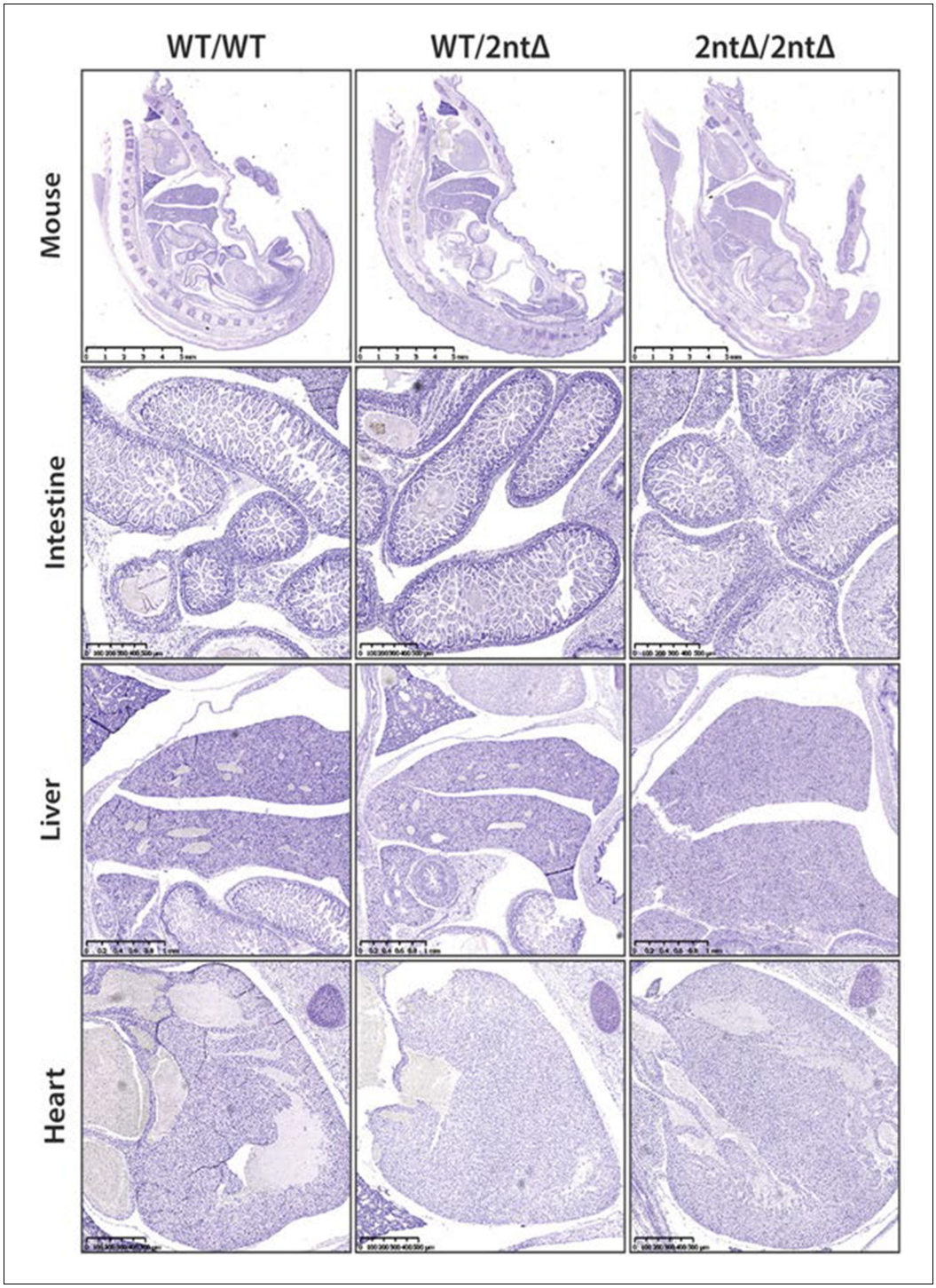

Figure 3—figure supplement 2. Ki-67 mutant mice develop normally. Sagittal sections of the whole mouse, intestine, liver and heart from WT *Mki67*$^{+/+}$ (WT/WT), heterozygous *Mki67*$^{+/2ntΔ}$(WT/2ntΔ) and homozygous *Mki67*$^{2ntΔ/2ntΔ}$(2ntΔ/2ntΔ) mice. Mouse sections, bar 5 mm; intestine sections, bar 500 μm; liver sections, bar 1 mm; heart sections, bar 500 μm.

DOI: 10.7554/eLife.13722.008

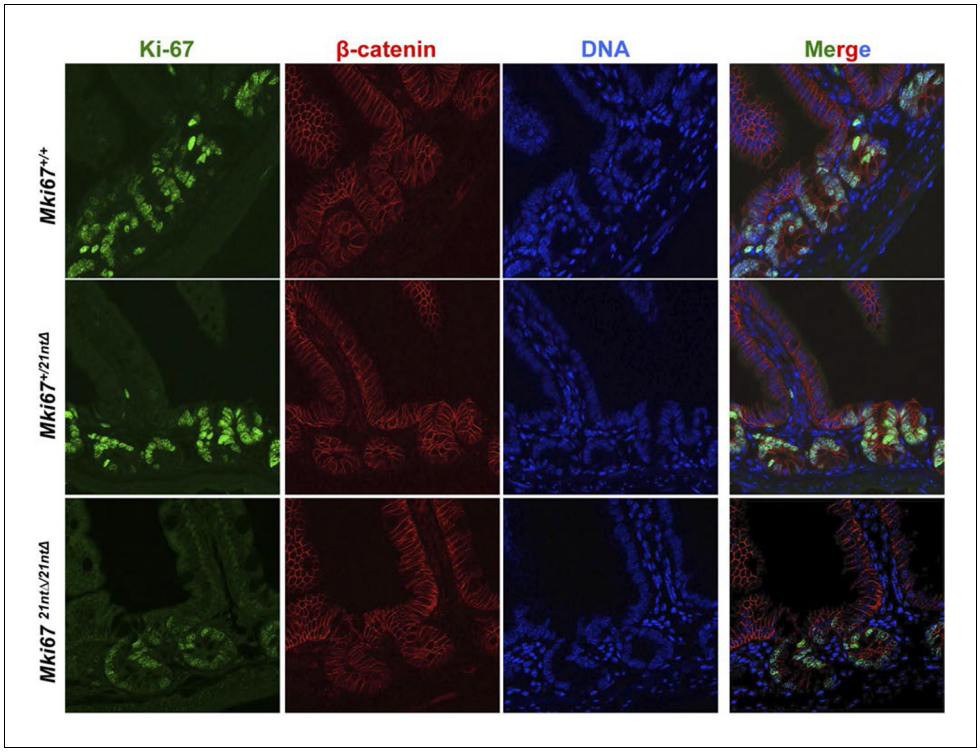

Figure 3—figure supplement 3. Background Ki-67 levels in Ki-67 mutant mice. Immunofluorescence of Ki-67 and β-catenin on sagittal sections of the mouse intestinal epithelium from *Mki67*$^{+/+}$, heterozygous *Mki67*$^{+/21nt\Delta}$and homozygous *Mki67*$^{21nt\Delta/21nt\Delta}$mice.

DOI: 10.7554/eLife.13722.009

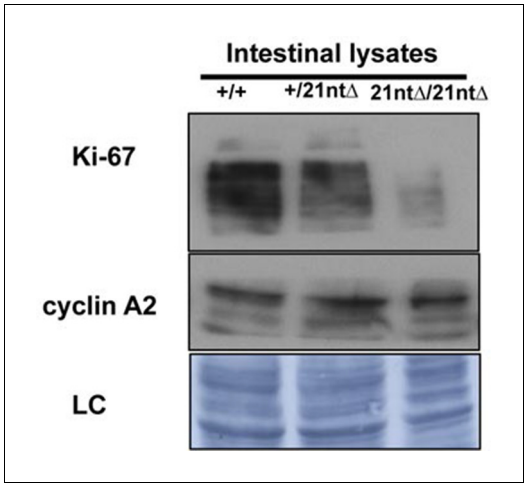

Figure 3—figure supplement 4. Background Ki-67 levels in Ki-67 mutant mice. Immunoblotting of Ki-67 and cyclin A on protein preparations of intestinal epithelium from *Mki67*$^{+/+}$ (+/+), heterozygous *Mki67*$^{+/21nt\Delta}$(+/21ntΔ) and homozygous *Mki67*$^{21nt\Delta/21nt\Delta}$(21ntΔ/21ntΔ) mice.

DOI: 10.7554/eLife.13722.010

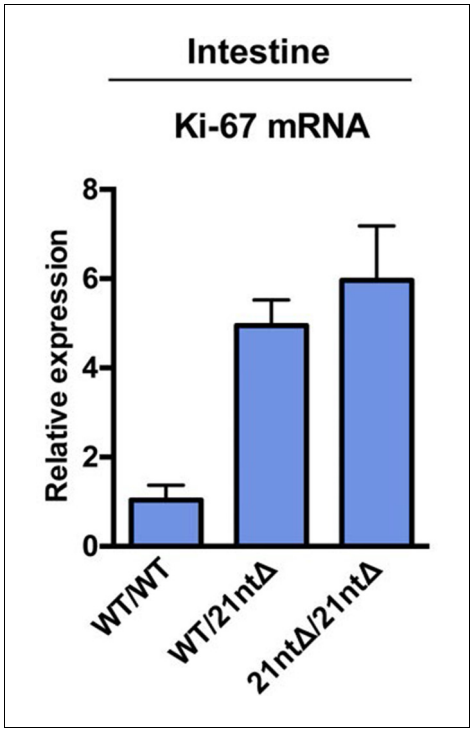

Figure 3—figure supplement 5. Ki-67 mRNA levels are not reduced in Ki-67 mutant mice. qRT-PCR of relative Ki-67 mRNA expression, normalised to GAPDH, on preparations of intestinal epithelium from *Mki67*$^{+/+}$ (WT/WT), heterozygous *Mki67*$^{+/21nt\Delta}$(WT/21ntΔ) and homozygous *Mki67*$^{21nt\Delta/21nt\Delta}$(21ntΔ/21ntΔ)mice.
DOI: 10.7554/eLife.13722.011

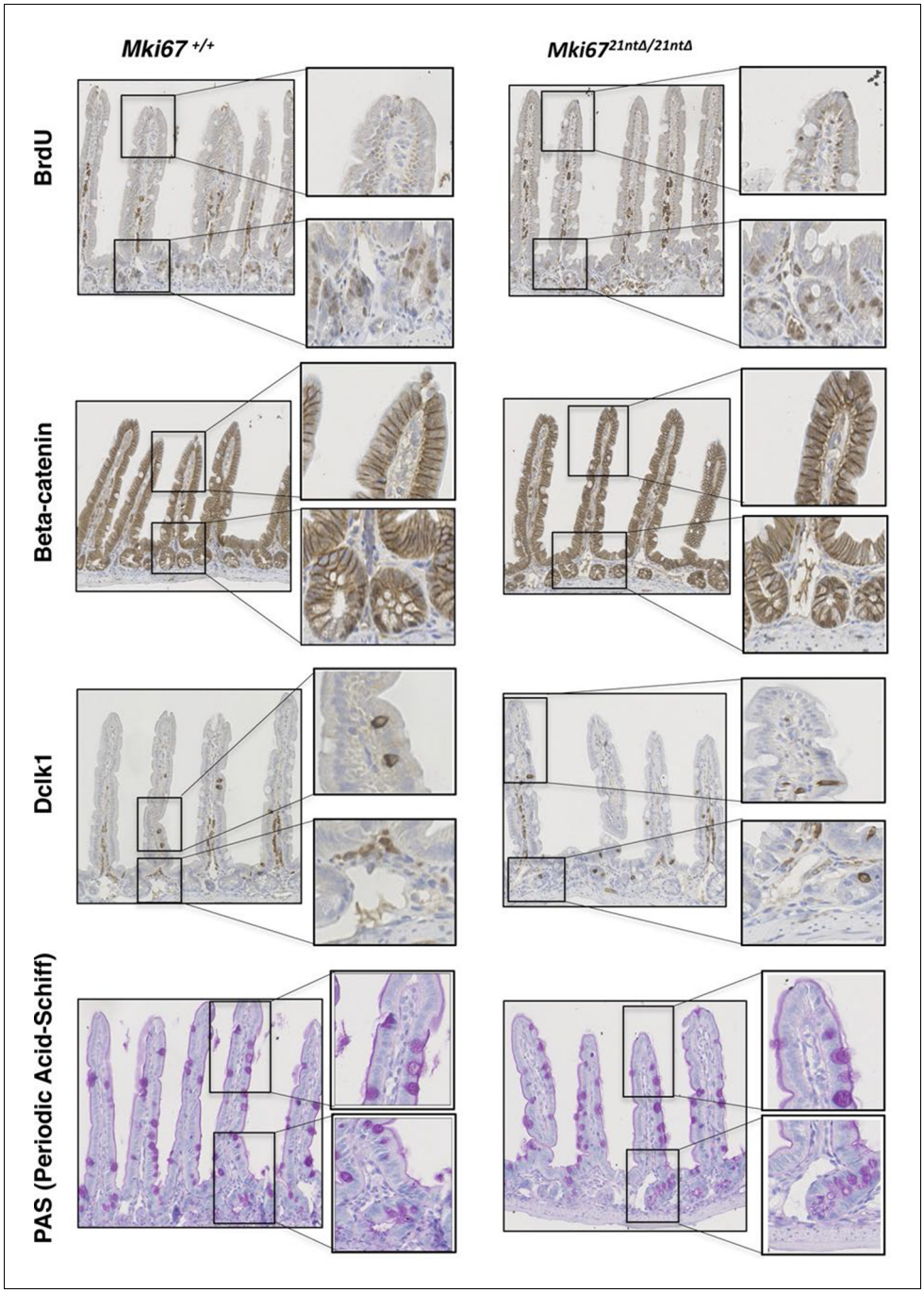

Figure 3—figure supplement 6. Normal proliferation and differentiation in Ki-67 mutant mice. Sagittal sections of the intestine from WT *Mki67*$^{+/+}$ and homozygous *Mki67*$^{21nt\Delta/21nt\Delta}$mice sacrificed after a 2 hr BrdU pulse, immunostained for BrdU, β-catenin, DCLK1 (a marker for tuft cells) or PAS staining of mucopolysaccharides (a marker for goblet cells).

DOI: 10.7554/eLife.13722.012

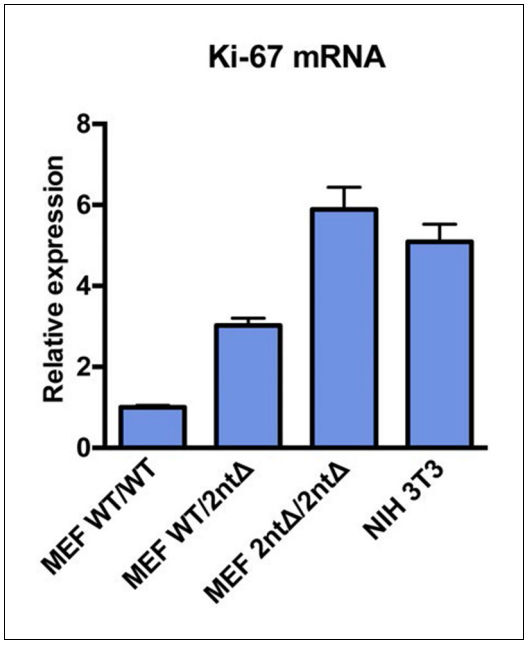

Figure 3—figure supplement 7. Ki-67 mRNA levels are not reduced in MEFs from Ki-67 mutant mice. qRT-PCR of relative Ki-67 mRNA expression, normalised to GAPDH, in MEFs isolated from *Mki67*$^{+/+}$ (WT/WT), heterozygous *Mki67*$^{+/2ntΔ}$(WT/2ntΔ) and homozygous *Mki67*$^{2ntΔ/2ntΔ}$(2ntΔ/2ntΔ)mice, compared to NIH3T3 cells.

DOI: 10.7554/eLife.13722.013

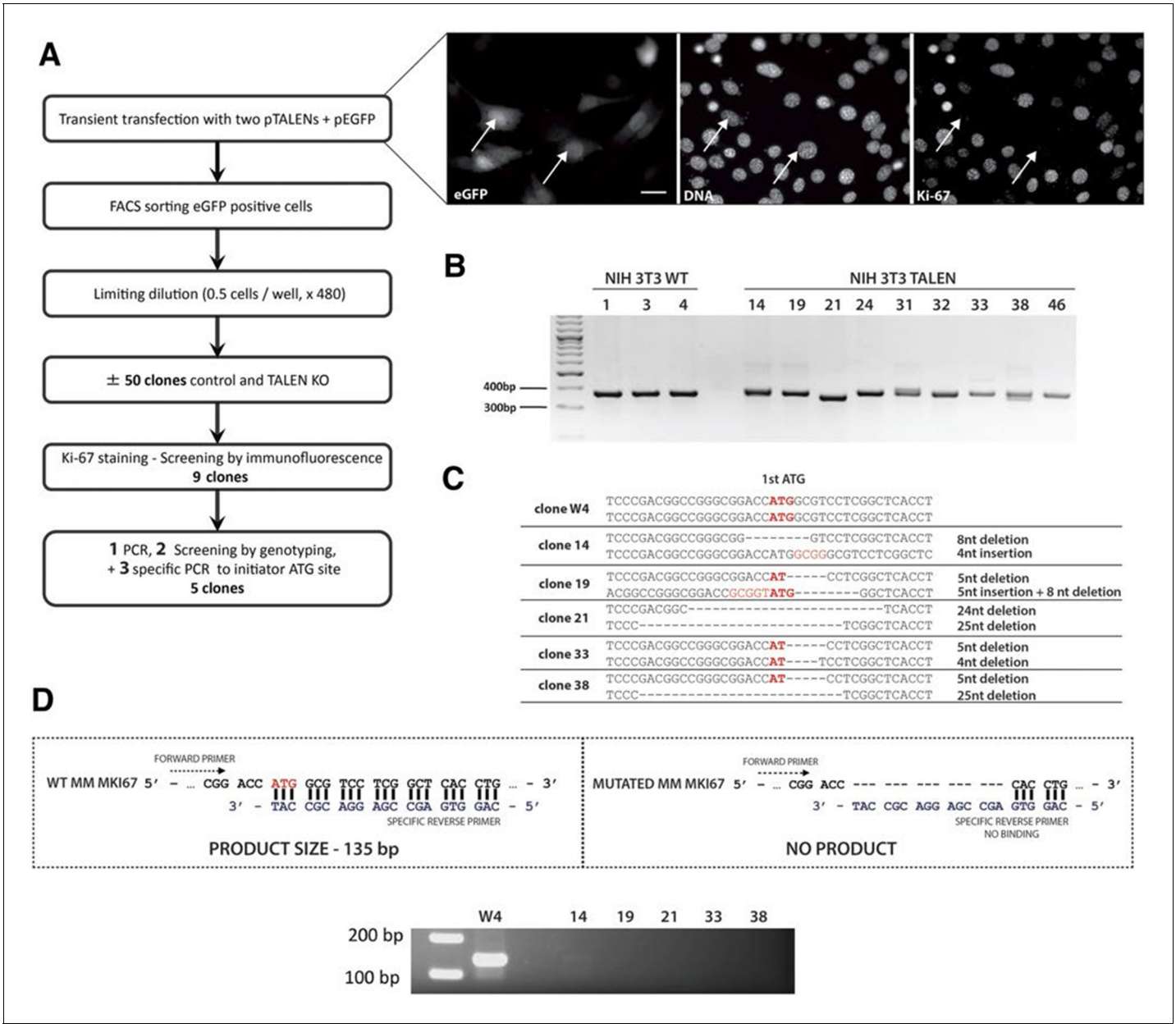

Figure 3—figure supplement 8. Generation of Ki-67-mutant NIH-3T3 cells. (**A**) Top and left, schematic representation of TALEN-mediated generation of NIH-3T3 biallelic Ki-67 mutant cells. Top right, immunofluorescence of Ki-67 and eGFP staining in NIH 3T3 cells transfected with two plasmids encoding TALEN pair and plasmid pEGFP. White arrows show Ki-67-negative pEGFP cotransfected cells. Scale bar 25 μm. (**B**) PCR analysis of *Mki67* initiator ATG surrounding sequence in genomic DNA prepared from three WT clones and nine Ki-67 immunofluorescence-negative clones selected for further analysis. (**C**) sequencing of *Mki67* initiator ATG area from selected clones (14, 19, 21, 33, 38). (**D**), PCR analysis targeted to the initiator ATG in *Mki67* gene of genomic DNA purified from NIH 3T3 WT clone W4 and Ki-67 KO clones 14, 19, 21, 33, 38.

DOI: 10.7554/eLife.13722.014

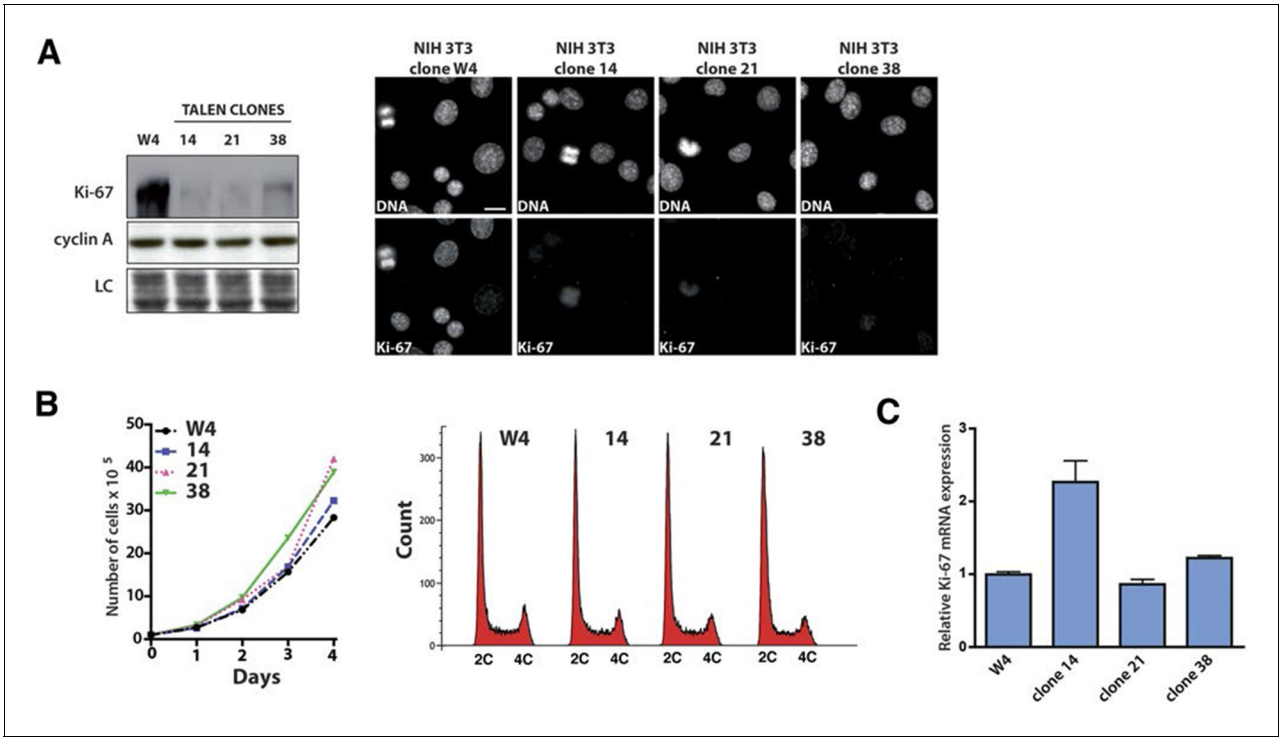

Figure 3—figure supplement 9. Ki-67-mutant NIH-3T3 cells proliferate normally. (**A**) Left, analysis of the indicated protein levels by Western blotting in NIH 3T3 WT clone 4 (W4) and Ki-67 mutant clones 14, 21 and 38. LC, loading control. (**B**) Left, growth curves of NIH 3T3 WT clone W4 and Ki-67 mutant clones 14, 21 and 38. NIH 3T3 WT and mutant cells were counted every day for 4 days. Right, cell cycle distribution of the WT clone W4 and 14, 21, 38 Ki67 mutant clones as analysed by FACS. (**C**) qRT-PCR analysis of Ki-67 mRNA in NIH 3T3 WT clone W4 and NIH Ki-67 mutant clones 14, 21 and 38. Normalized by mRNA expression of *B2m* (beta-2-microglobulin).

DOI: 10.7554/eLife.13722.015

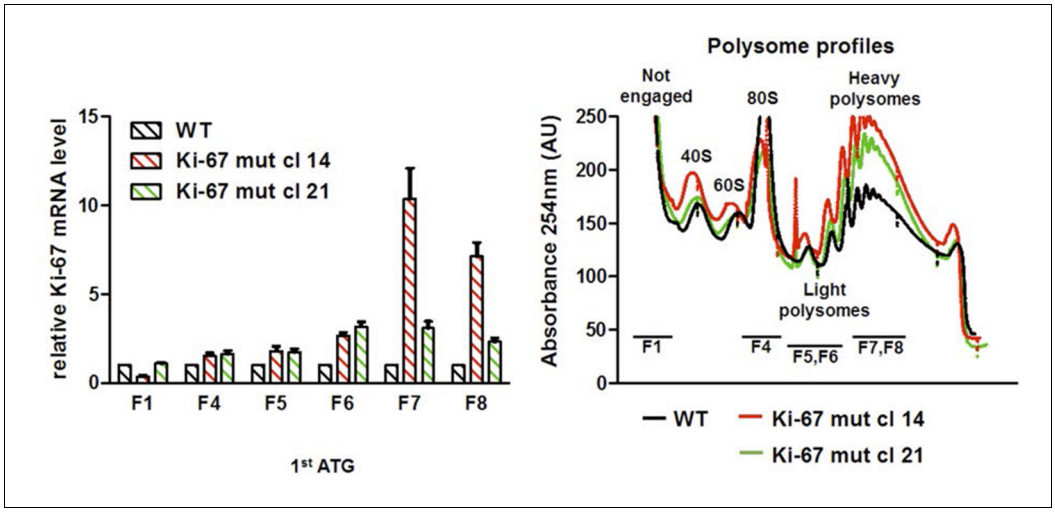

Figure 3—figure supplement 10. Basal translation of Ki-67 with a mutated ATG. Left: quantification of association of Ki-67 mRNA with ribosome fractions in biallelic single TALEN Ki-67 mutant NIH-3T3 cells by qRT-PCR, normalised to GAPDH, b2-microglobulin and actin mRNA and to WT levels. Right: RNA quantification of fractions by spectrophotometric absorbance at 254 nm.

DOI: 10.7554/eLife.13722.016

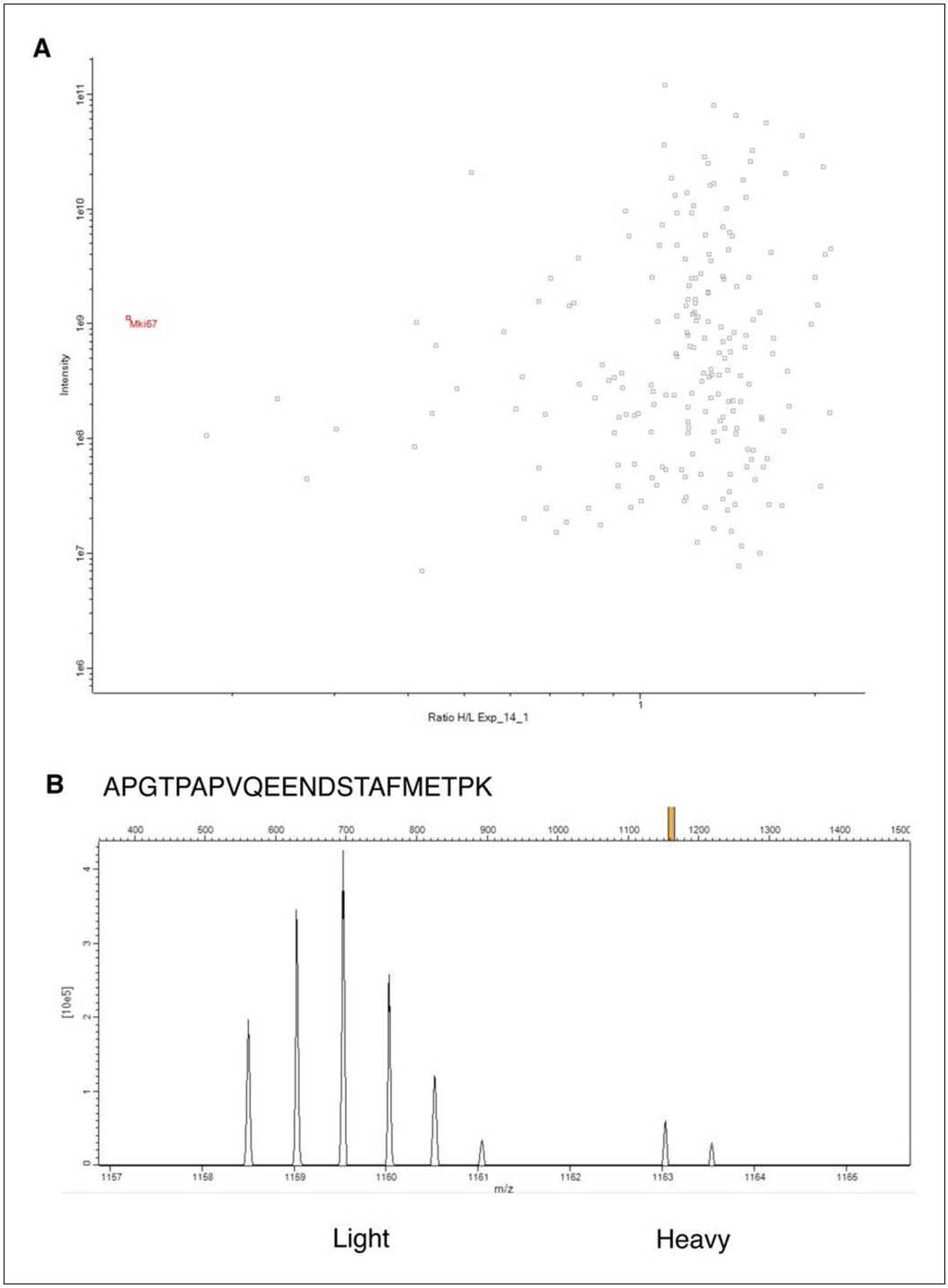

Figure 3—figure supplement 11. SILAC proteomics analysis of Ki-67 expression with a mutated ATG. (**A**) Scatterplot showing H/L m/z peak ratios (x-axis) against intensity levels (y-axis) from band 1 of SDS-PAGE purified chromatin, where H-labelled samples were Ki-67 mutant NIH-3T3 clone 14, L samples were W4 wild-type control. Most proteins have unaltered expression between the two cell lines (H/L ratio ≈ 1). Average H/L ratio of putative Ki-67 peptides (predicted by Maxquant on the basis of isotope profiles with the expected difference in m/z ratio from Ki-67 L-peptides positively identified by MS/MS) is shown in red. (**B**) Isotope profile of a light Ki-67 peptide from control cell chromatin identified by MS/MS, and the corresponding heavy peaks used for quantification. Data is provided in ***Figure 3—figure supplement 11—source data 1***.

DOI: 10.7554/eLife.13722.017

Figure 3—figure supplement 11 continued on next page

Figure 3—figure supplement 11 continued

The following source data is available for figure 3:

Figure supplement 11—Source data 1. SILAC quantitation of Ki-67 peptides from WT and Mki67-mutant NIH-3T3 cells.

DOI: 10.7554/eLife.13722.018

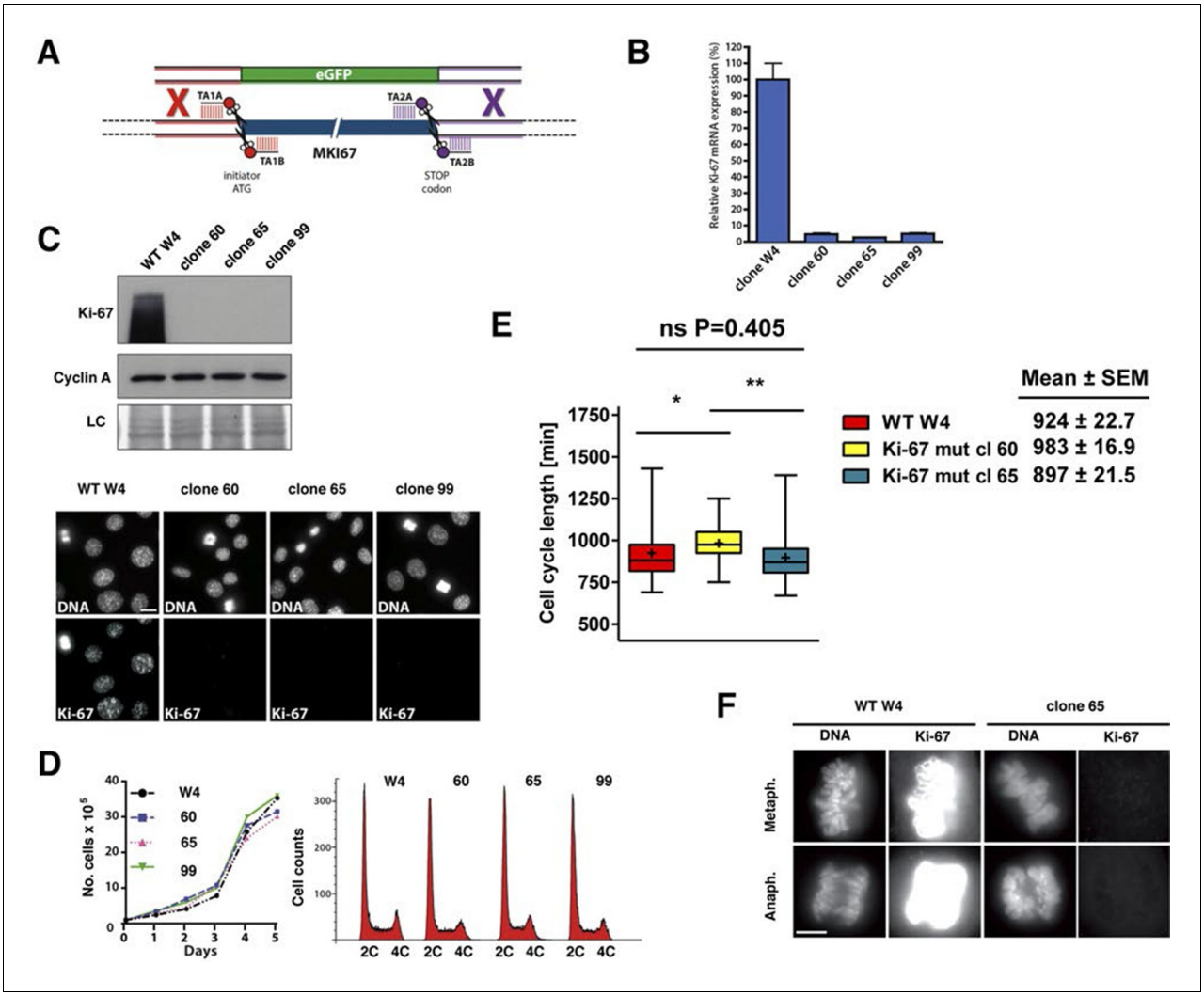

Figure 4. Cell proliferation without Ki-67. (**A**) Schematic representation of strategy for TALEN-mediated generation of *Mki67* null allele. (**B**) qRT-PCR analysis of Ki-67 mRNA levels in NIH-3T3 WT clone W4 and Ki-67-negative 60, 65, 99 clones. (**C**) Top: Western blot of Ki-67 and Cyclin A in NIH-3T3 WT clone W4 and Ki-67-negative mutant clones 60, 65, 99; LC, loading control; below, Ki-67 immunofluorescence; bar, 10 μm. (**D**) Left, growth curves of WT and Ki-67 null cell lines 60, 65 and 99; right, cell cycle distribution analysed by flow cytometry. (**E**) Cell cycle length of WT clone W4 and Ki-67 null clones 60 and 65 as determined by time-lapse videomicroscopy. (**F**) Cells of clone 65 show altered chromosomal periphery in mitosis. The Ki-67 staining is deliberately overexposed to demonstrate absence of detectable Ki-67 in clone 65, even in metaphase. Bar, 5 μm.

DOI: 10.7554/eLife.13722.019

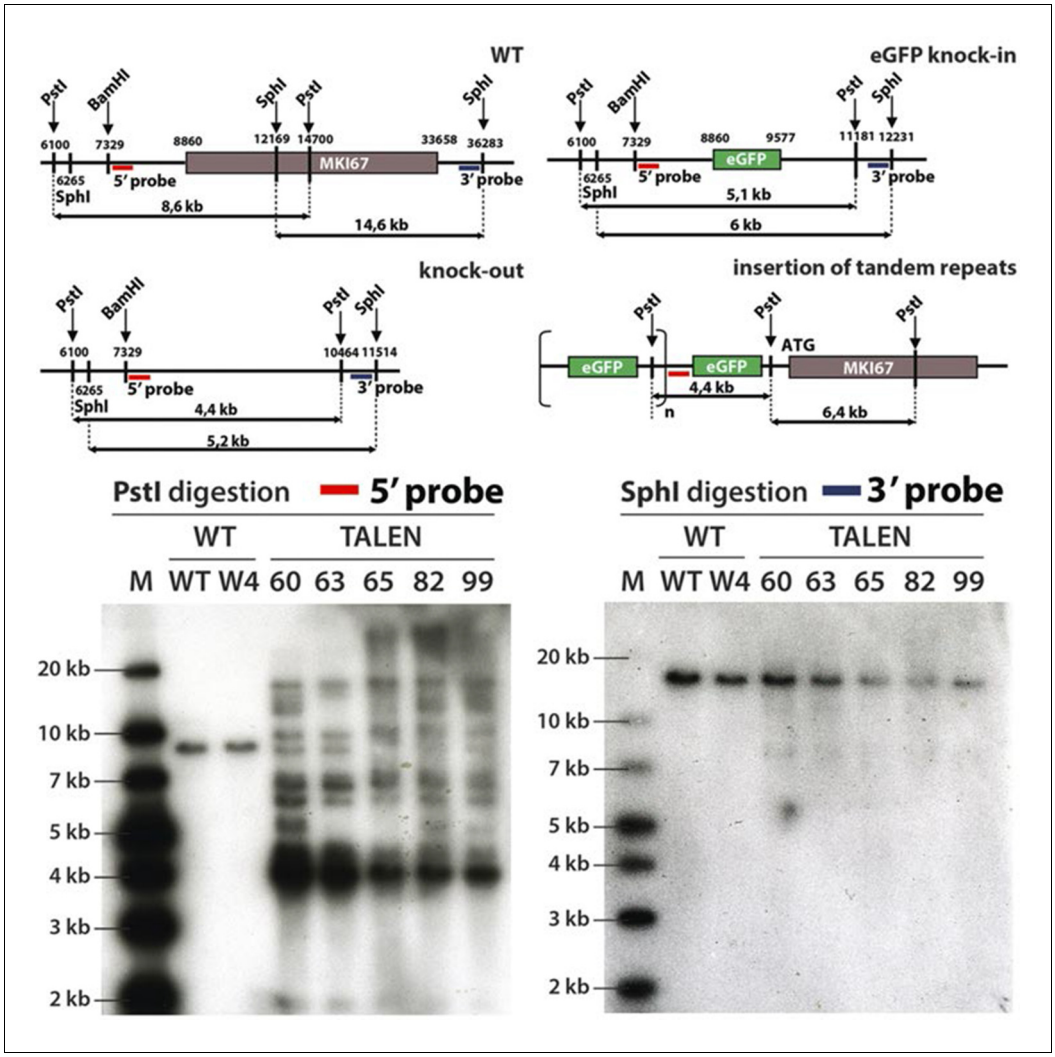

Figure 4—figure supplement 1. Generation of NIH-3T3 cells lacking Ki-67. Top, schematic representation of the wild type (WT), knock-out or eGFP knock-in *Mki67* locus and the predicted insertion of tandem repeats of the eGFP insert upstream of *Mki67* locus. Bottom, Southern-blot of two NIH-3T3 WT clones (WT, W4) and six NIH-3T3 Ki-67 mutant clones (60,63,65,82,99). Clones were digested with PstI or SphI and probed with 5' or 3' probe, respectively.

DOI: 10.7554/eLife.13722.020

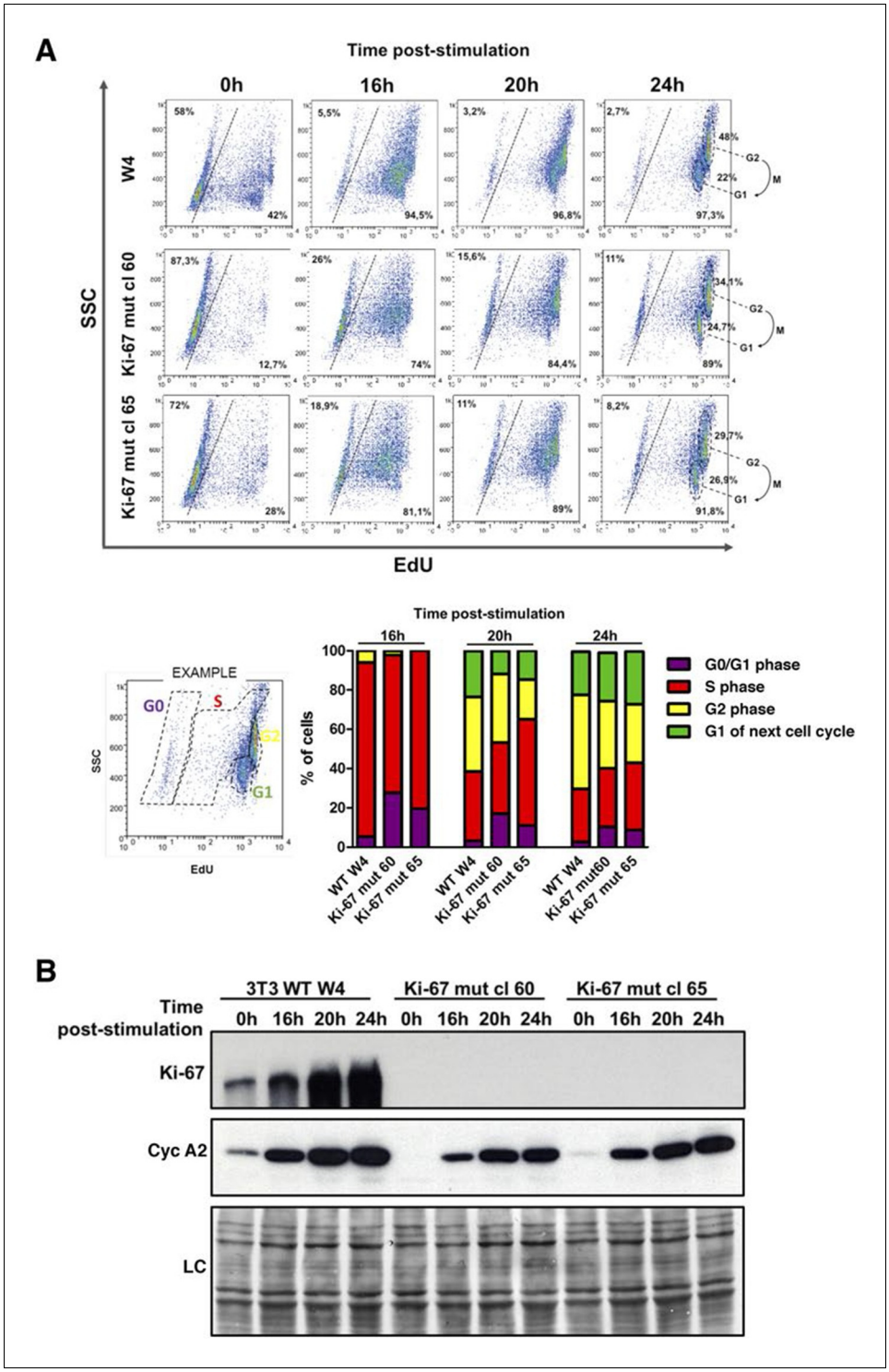

Figure 5. Cells lacking Ki-67 enter the cell cycle efficiently. (**A**) Top, re-entry of cell cycle in NIH-3T3 WT clone W4 and Ki-67-negative mutant clones 60 and 65 after serum starvation-induced cell cycle arrest. Progression of cell cycle entry analysed by FACS using EdU staining. Bottom, quantification of cell cycle phases in this experiment. (**B**) Western blot analysis of Ki-67 (upper panel) and cyclin A2 (lower panel) upon cell cycle entry. LC, loading control.
DOI: 10.7554/eLife.13722.021

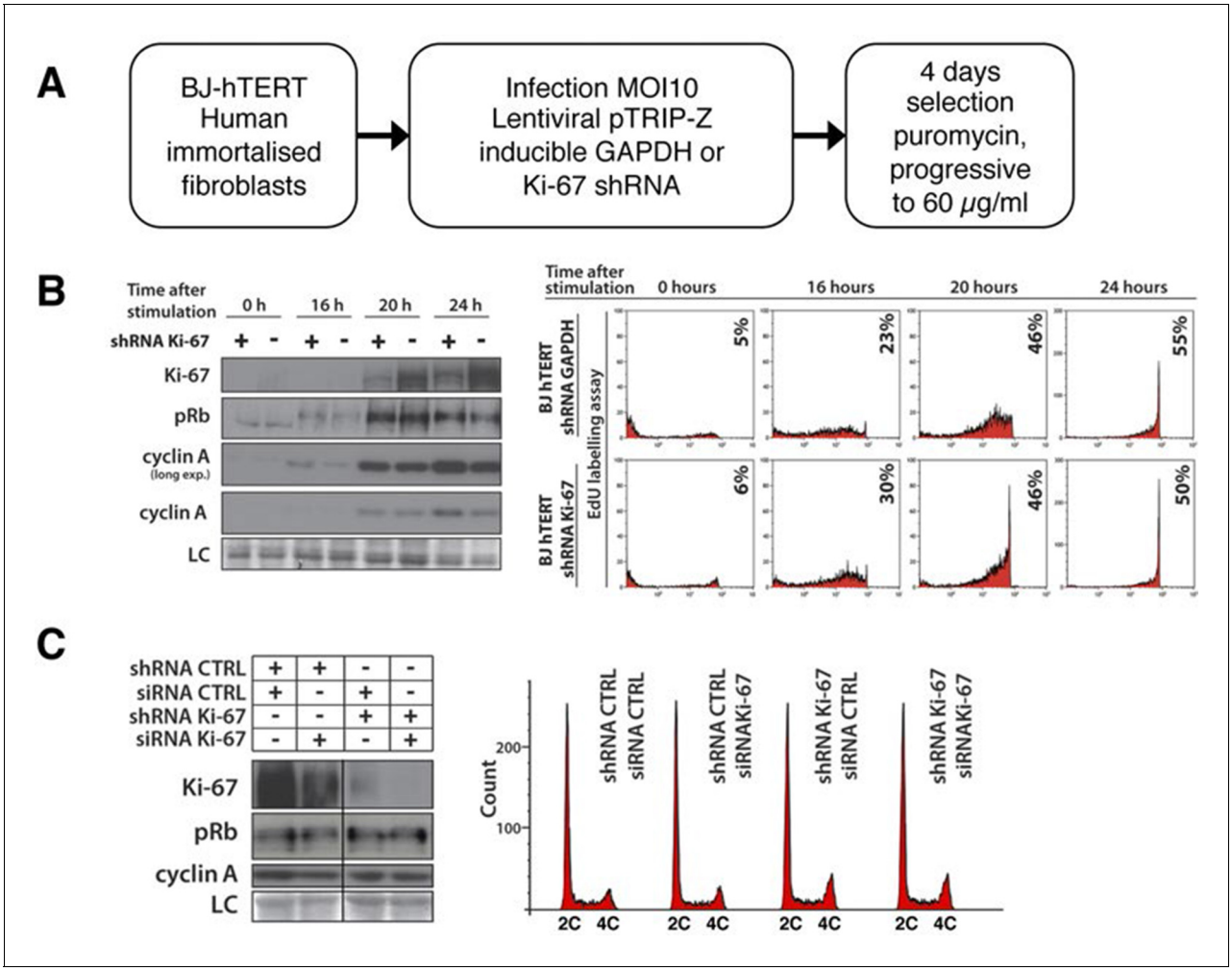

Figure 5—figure supplement 1. Cells lacking Ki-67 proliferate efficiently. (**A**) Schematic presentation of generation of Ki-67 shRNA knockdown BJ-hTERT. (**B**) Left, Western blot for indicated proteins upon cell cycle re-entry in serum starved hTERT-transformed BJ fibroblasts (BJ-hTERT) after induction of shRNA against Ki-67 (+) or GAPDH control (-). LC, loading control. Right, DNA synthesis analysed by flow cytometry after EdU pulse. (**C**) Left, asynchronous BJ-hTERT with doxycyclin-induced control or Ki-67 shRNA-expression were additionally transfected with control or Ki-67 siRNA for 48 hr. Protein levels were analysed by Western blotting. LC, loading control. Right, cell cycle distribution by flow cytometry.
DOI: 10.7554/eLife.13722.022

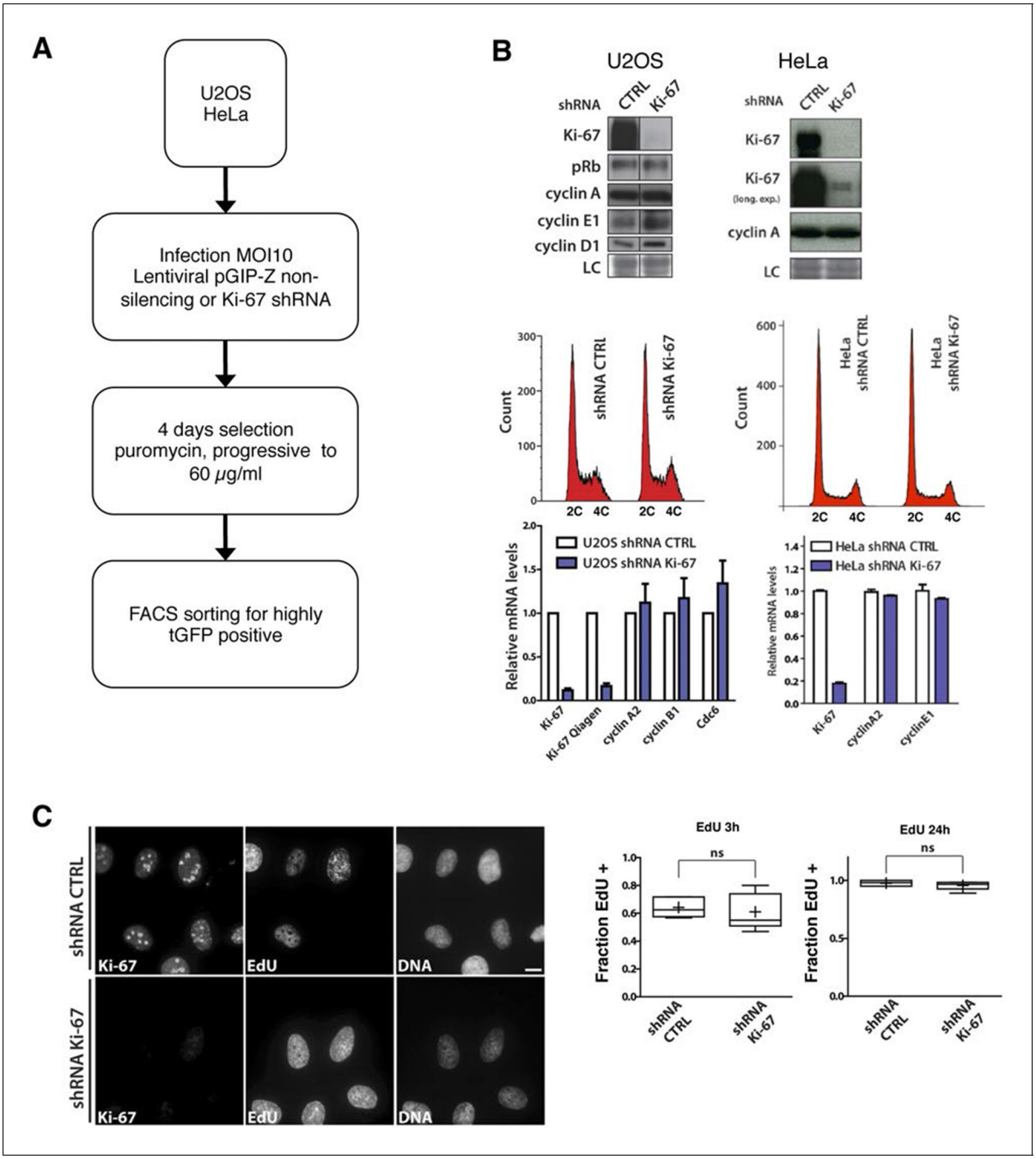

Figure 5—figure supplement 2. Cells lacking Ki-67 proliferate efficiently. (**A**) Schematic presentation of generation of Ki-67 shRNA knockdown cell lines. (**B**) Top: Western blot analysis of the indicated proteins in asynchronously growing U2OS and HeLa cells stably expressing non-targeting (CTRL) or Ki-67 shRNA. Lanes separated by lines were from a single exposure of a single SDS-PAGE gel and Western blot. LC, loading control. Middle: Cell cycle distribution of these cells. Bottom: qRT-PCR analysis of the indicated mRNA levels, normalized by mRNA expression of beta-2-microglobulin (*B2m*). (**C**) Immunofluorescence of Ki-67 and EdU in asynchronous U2OS cells stably expressing control or Ki-67 shRNA, incubated with 5-ethynyl-2'-deoxyuridine (EdU) for 3 hr. Bar, 10 μm. Right: Ratio of EdU-positive cells to the total cell number for each incubation time; ns: not significant.

DOI: 10.7554/eLife.13722.023

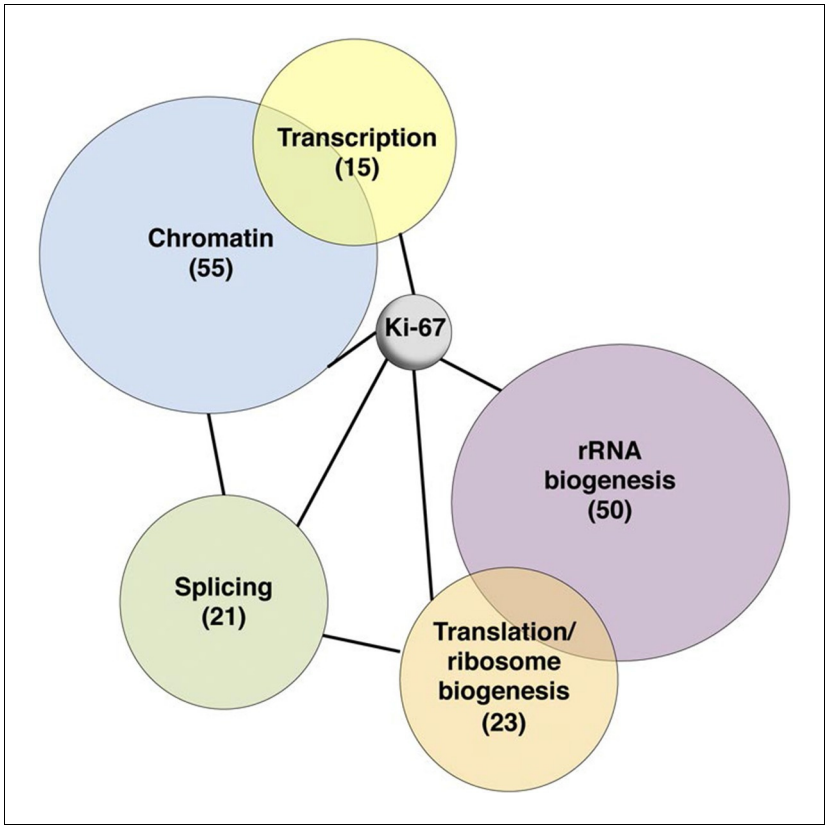

Figure 6. Ki-67 interacts with proteins involved in nucleolar processes and chromatin. Simplified STRING analysis reveals network interactions between proteins associating with Ki-67. The full network is shown in ***Figure 6—figure supplement 2***; data is provided in ***Figure 6—source data 1***.

DOI: 10.7554/eLife.13722.024

The following source data is available for figure 6:

Source data 1. Ki-67 interacting proteome.

DOI: 10.7554/eLife.13722.025

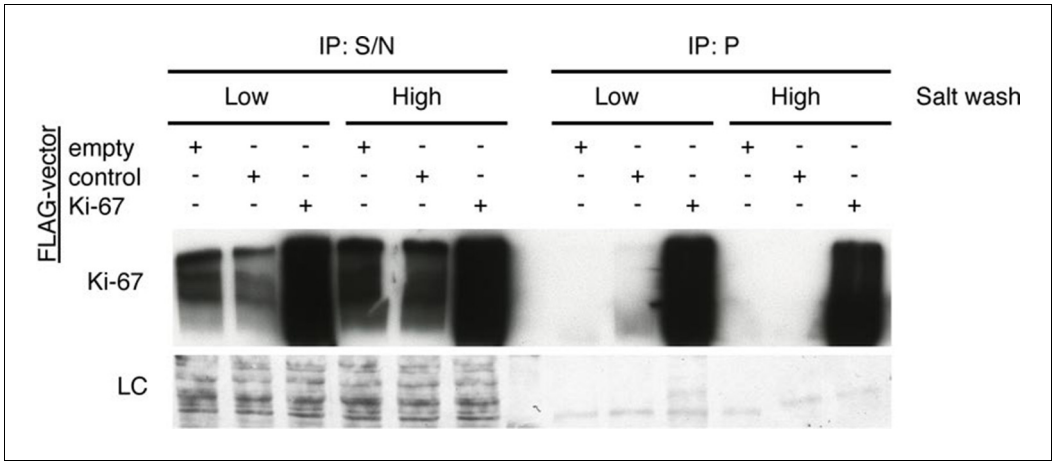

Figure 6—figure supplement 1. The Ki-67 interactome. Western blot of Ki-67 in nuclear extracts from cells expressing FLAG-tagged versions of Ki-67 or a control unrelated protein, or FLAG alone. IP: immunoprecipitation; S/N: supernatant; P: pellet. Bottom, loading control.

DOI: 10.7554/eLife.13722.026

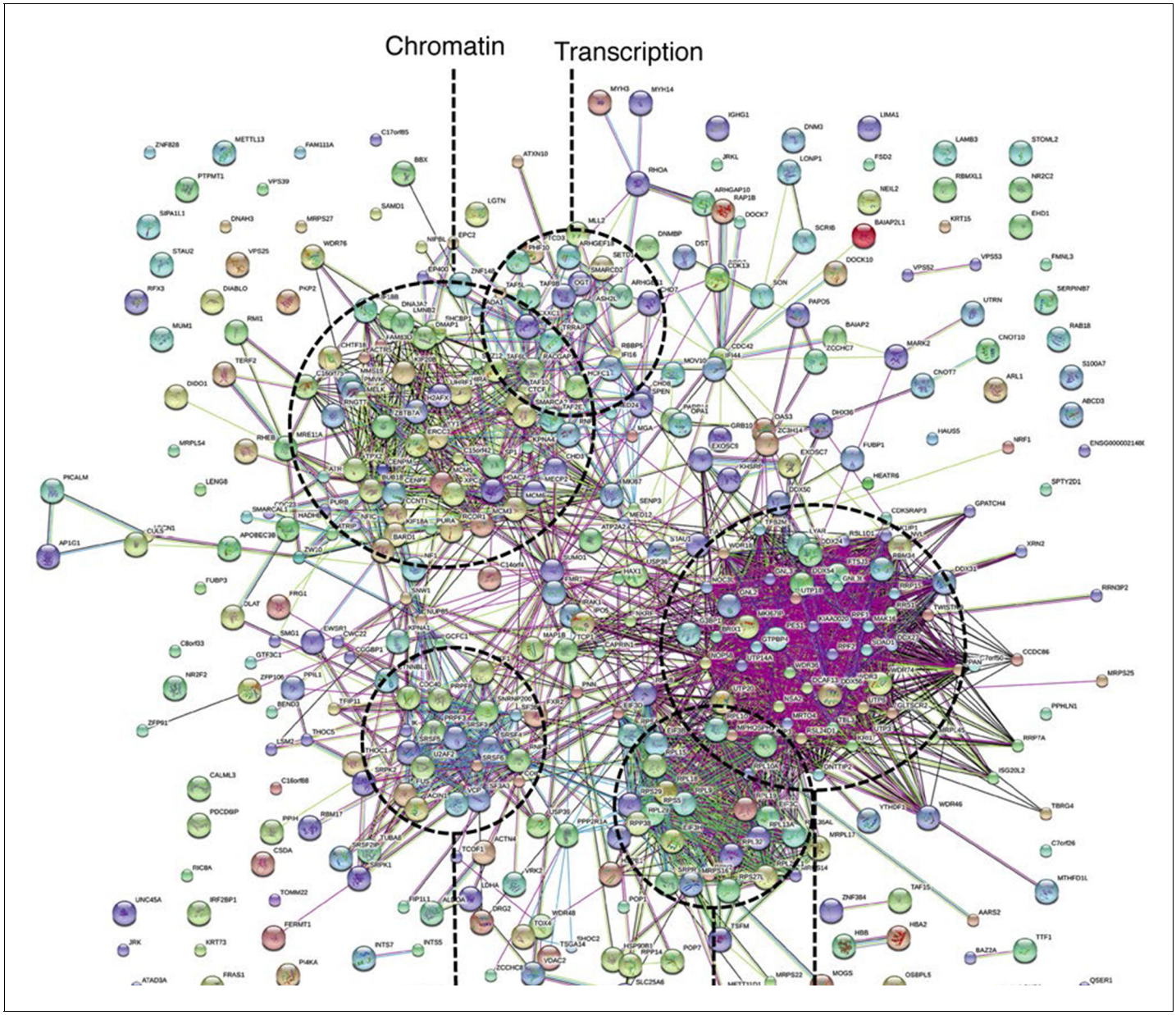

Figure 6—figure supplement 2. Ki-67 interacts with proteins involved in nucleolar processes and chromatin. STRING analysis of network interactions between proteins specifically associating with Ki-67 as identified by immunoprecipitation and mass spectrometry from U2OS cells expressing FLAG-tagged full length human Ki-67.

DOI: 10.7554/eLife.13722.027

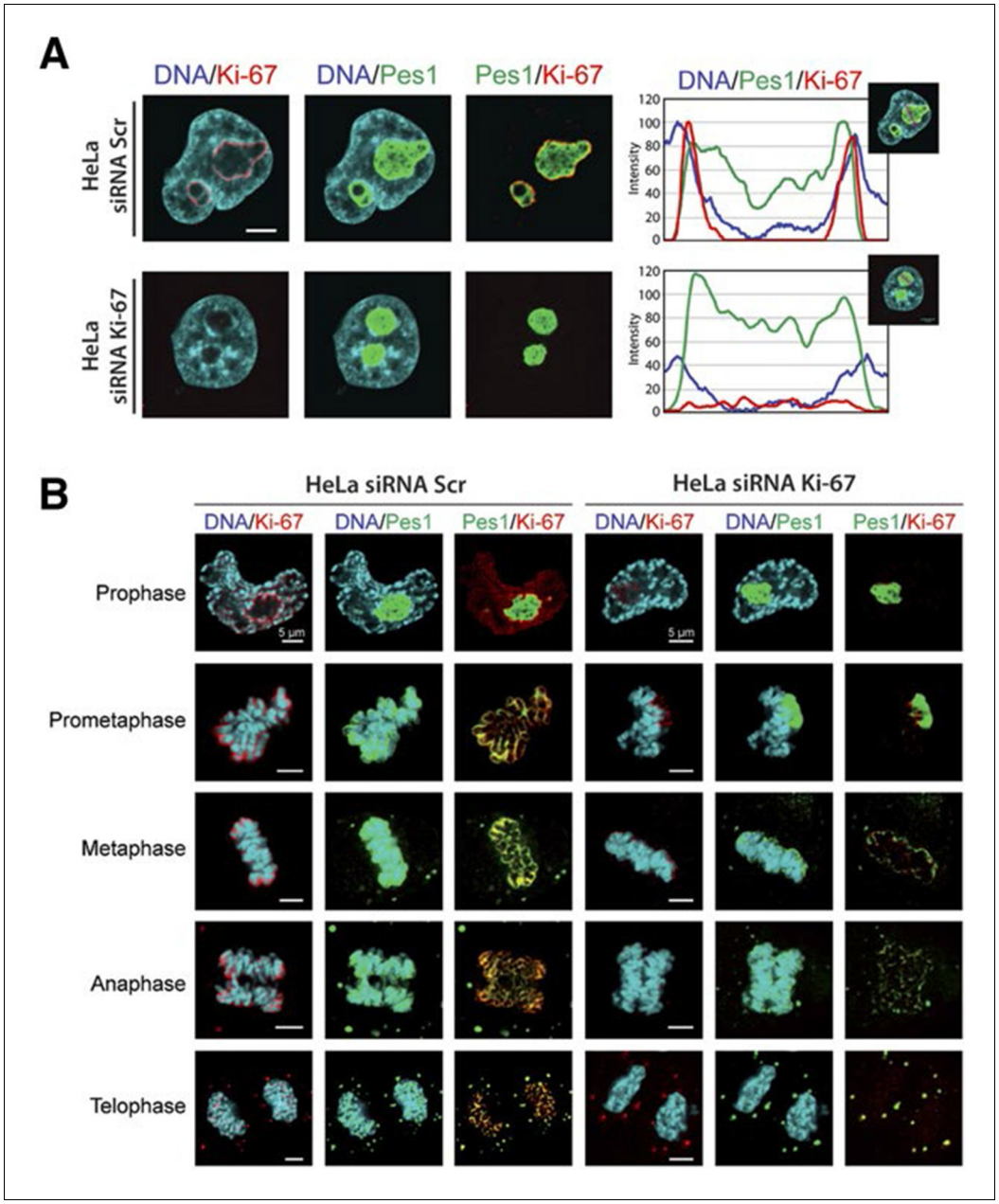

Figure 7. Ki-67 localises PES1 to mitotic chromosomes. (**A**) Analysis of the interphase localisation of PES1 and Ki-67 proteins by immunofluorescence in HeLa cells 72 hr after transfection with control siRNA (scramble; Scr) or Ki-67 RNAi. Right, line scans showing the distribution of fluorescence signals within indicated nucleoli (dashed line). Images were captured in confocal mode with a spinning-disk microscope. Bar, 5 µm. (**B**) Analysis of the mitotic localisation of PES1 and Ki-67 proteins by immunofluorescence in HeLa cells 72 hr after transfection with control siRNA (scramble; Scr) or Ki-67 RNAi. Bar, 5 µm.

DOI: 10.7554/eLife.13722.028

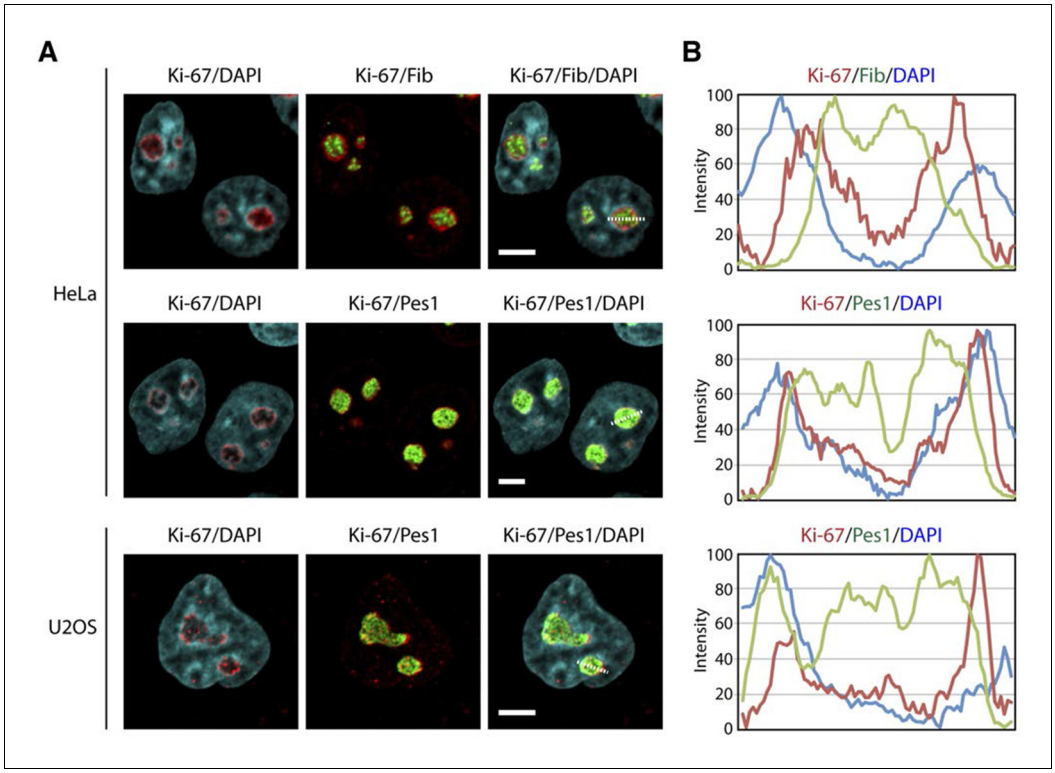

Figure 7—figure supplement 1. Ki-67 is a nucleolar protein localizing in the cortical side of the GC. (**A**) Localisation of Ki-67 protein by immunofluorescence in HeLa and U2OS cells. Fibrillarin (DFC) or Pes1 (GC) were used as nucleolar markers. Images were captured in confocal mode with a spinning-disk microscope. Objective 100 x. Scale bar: 5 µm. (**B**) Line scans showing the distribution of fluorescence signals within specific nucleoli (see dotted lines in panel A).

DOI: 10.7554/eLife.13722.029

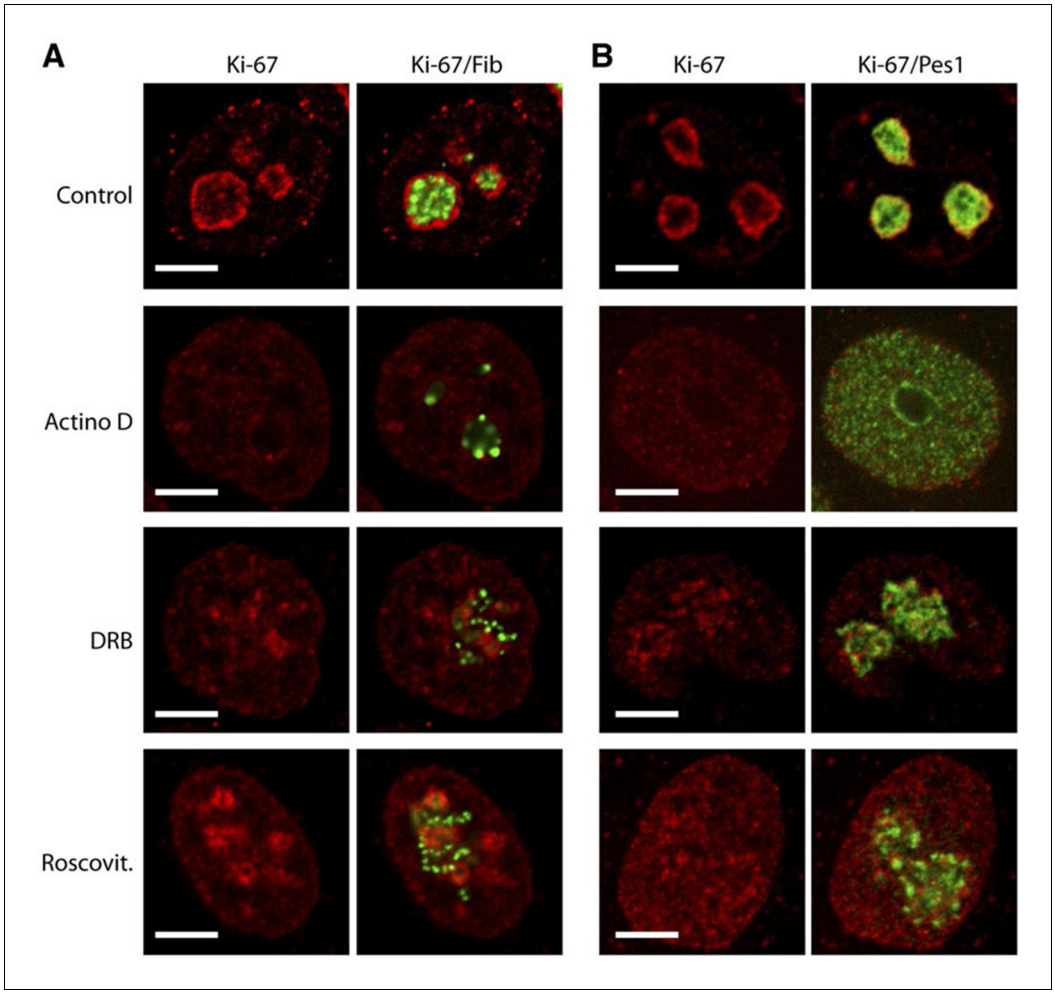

Figure 7—figure supplement 2. Ki-67 follows GC components upon drug-induced nucleolar disruption. Actinomycin D or the kinase inhibitors DRB and Roscovitine were added to cells during 90 min and Ki-67 was located within these cells by immunofluorescence. Fibrillarin (**A**) and PES1 (**B**) proteins were also localised by immunofluorescence. Objective 100 x. Scale bar: 5 μm.

DOI: 10.7554/eLife.13722.030

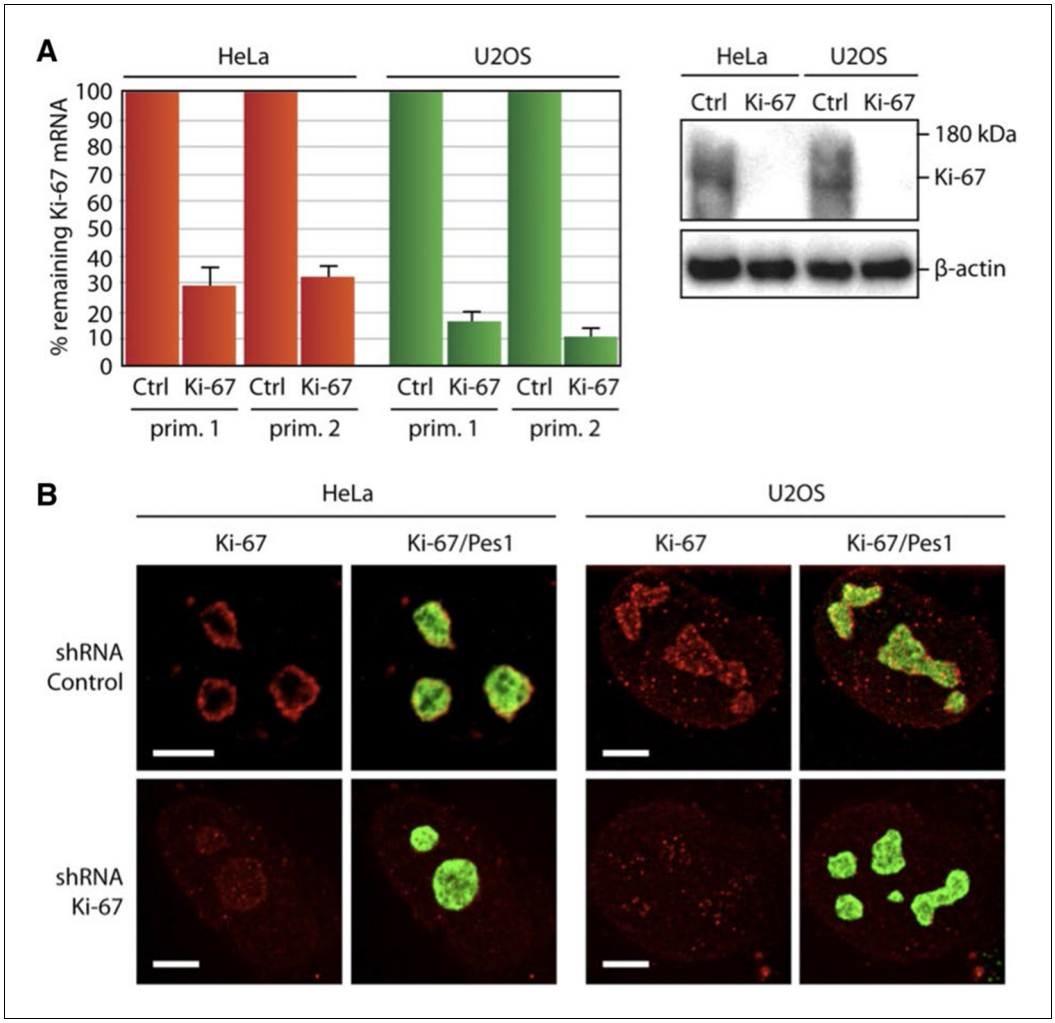

Figure 7—figure supplement 3. Depletion of Ki-67 does not affect overall nucleolar structure. (**A**) Histograms showing the level of Ki-67 mRNA remaining in the cell lines expressing constitutively the shRNA against Ki-67. These levels were assessed by RT-qPCR using two different pairs of primers. Right, the Western-blot against Ki-67 shows a disappearance of a bands in the cell lines constitutively expressing the shRNA against Ki-67. (**B**) Immunofluorescence against Ki-67 in control HeLa and U20S cell lines in the absence (control) or in the presence (Ki-67) of the shRNA targeting Ki-67 mRNA. The PES1 signal shows that the nucleolar structure is maintained. Objective 100 x. Scale bar: 5 μm.

DOI: 10.7554/eLife.13722.031

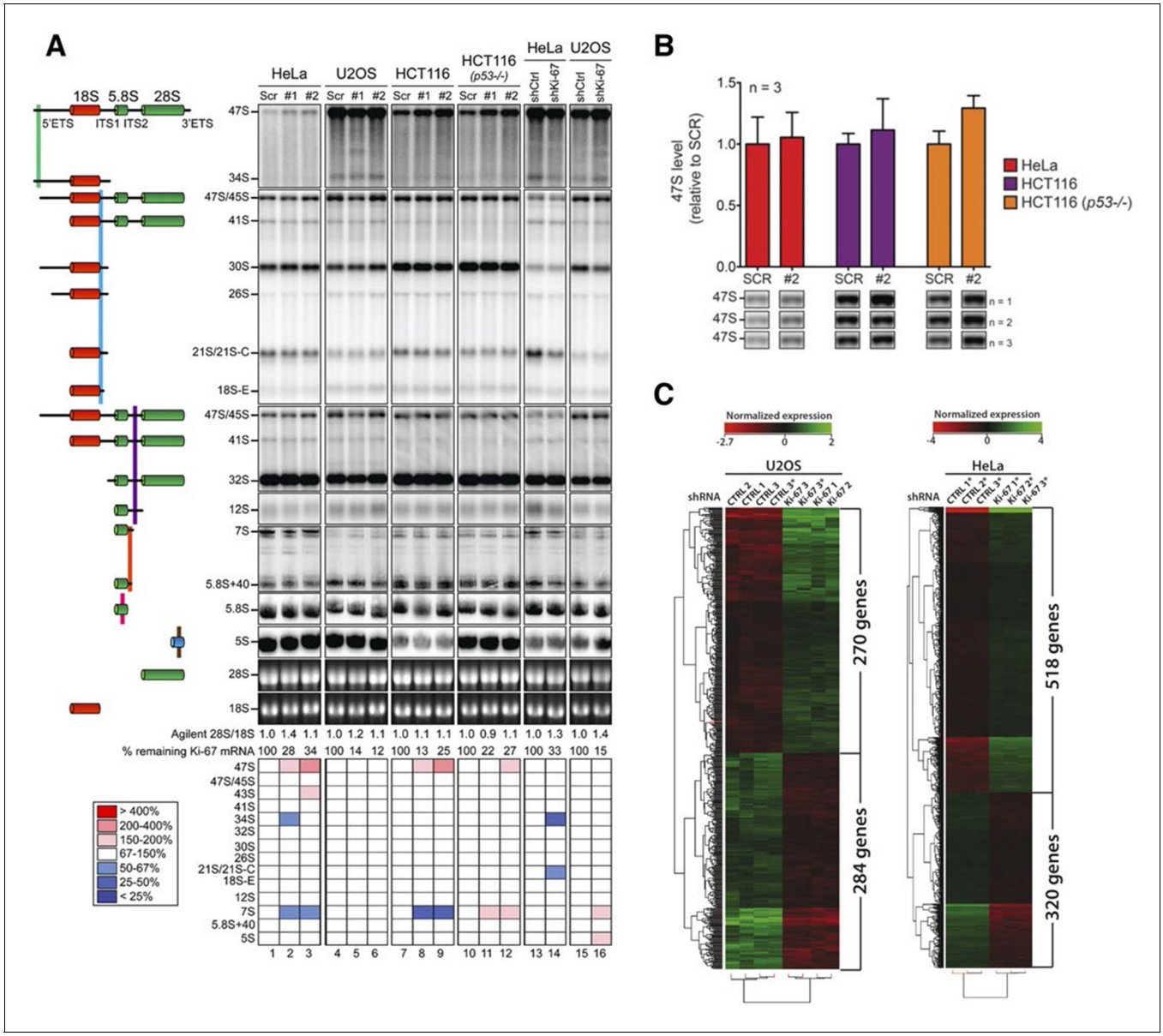

Figure 8. Ki-67 is not required for rRNA biogenesis but controls gene transcription. (**A**) Northern-blot analysis of total RNA extracted from HeLa and U2OS cells constitutively expressing shRNA against Ki-67; and HeLa, U2OS, HCT-116 and HCT-116 TP53 (-/-) depleted of Ki-67 by siRNA for 72 hr in two biological replicates (#1 and #2) or with scrambled siRNA control (Scr). Pre-rRNA intermediates were analysed by probing with different primers located in the different spacers of the 47S sequence (5'ETS-green; ITS1-blue; ITS2-purple). (B) Quantification of 47S rRNA precursor in HeLa, HCT-116 and HCT-116 TP53 (-/-) depleted of Ki-67 by siRNA for 72 hr in three biological replicates (n=1–3). (C) U2OS cells (left) or HeLa cells (right) show transcriptome profile differences (fold change >1.5; corrected p-value <0.02) between asynchronous cells constitutively expressing control (CTRL) or Ki-67 shRNA. Heat-maps present the expression levels of differentially expressed genes between biological replicates (1,2,3) and technical replicates (3, 3*). Data is provided in ***Figure 8—source data 1*** and ***2***.

DOI: 10.7554/eLife.13722.032

The following source data is available for figure 8:

Source data 1. Ki-67-dependent transcriptome in U2OS cells.

DOI: 10.7554/eLife.13722.033

Source data 2. Ki-67-dependent transcriptome in HeLa cells.

DOI: 10.7554/eLife.13722.034

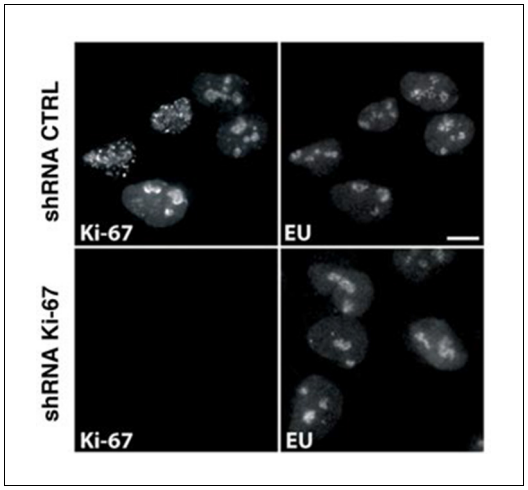

Figure 8—figure supplement 1. Ki-67 depletion does not hinder rRNA transcription. Newly synthesised RNA in asynchronous U2OS cells expressing control or Ki-67 shRNA visualised by 5-ethynyl uridine (EU) incorporation and immunofluorescence. Bar, 10 μm.
DOI: 10.7554/eLife.13722.035

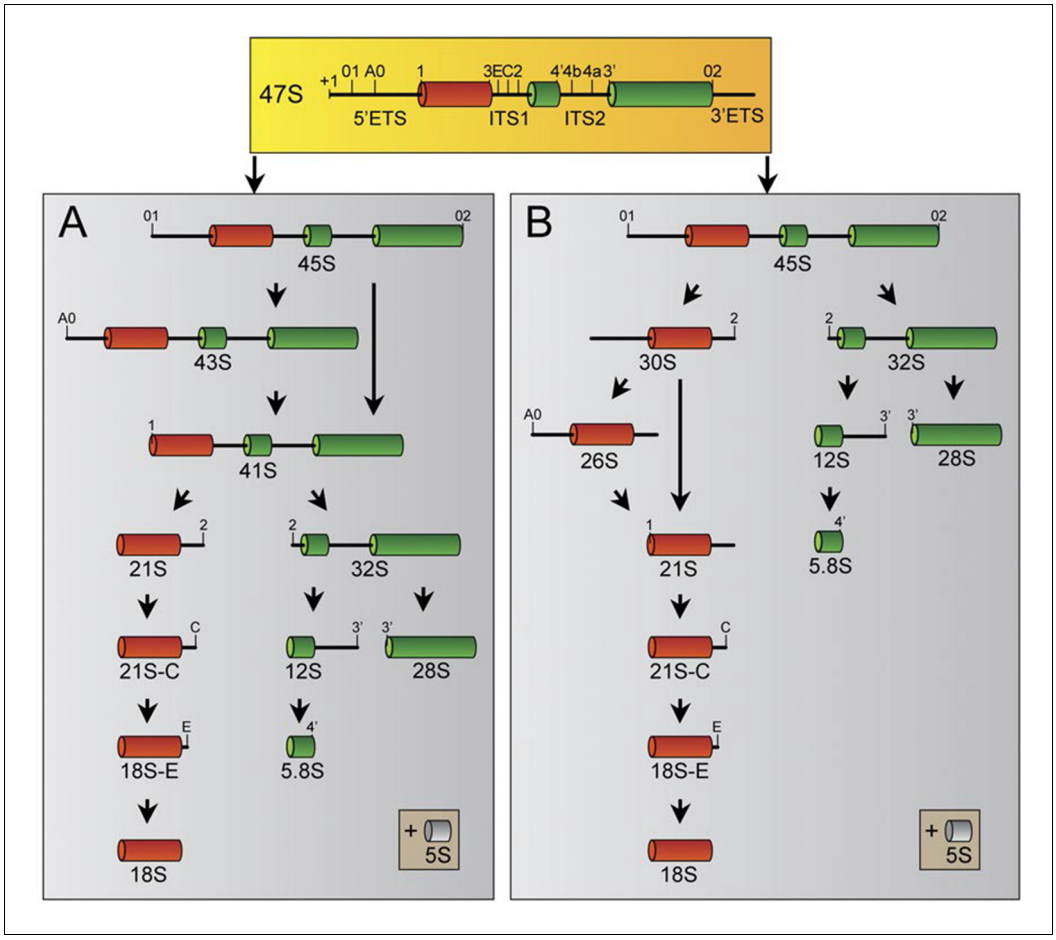

Figure 8—figure supplement 2. Human pre-rRNA processing pathway involves two major pathways. The two pathways (**A** and **B**) are characterized by specific cleavage kinetics. In pathway A, cleavages at the site A0 and 1 occur before cleavage at the site 2, whereas cleavage at site 2 occurs before cleavages at sites A0 and 1 in the pathway B. Both pathways will end by the production of the mature 28S, 18S and 5.8S. The 5S rRNA is synthesized by the RNA pol III in the nucleoplasm and will join the other rRNAs during ribosome assembly.

DOI: 10.7554/eLife.13722.036

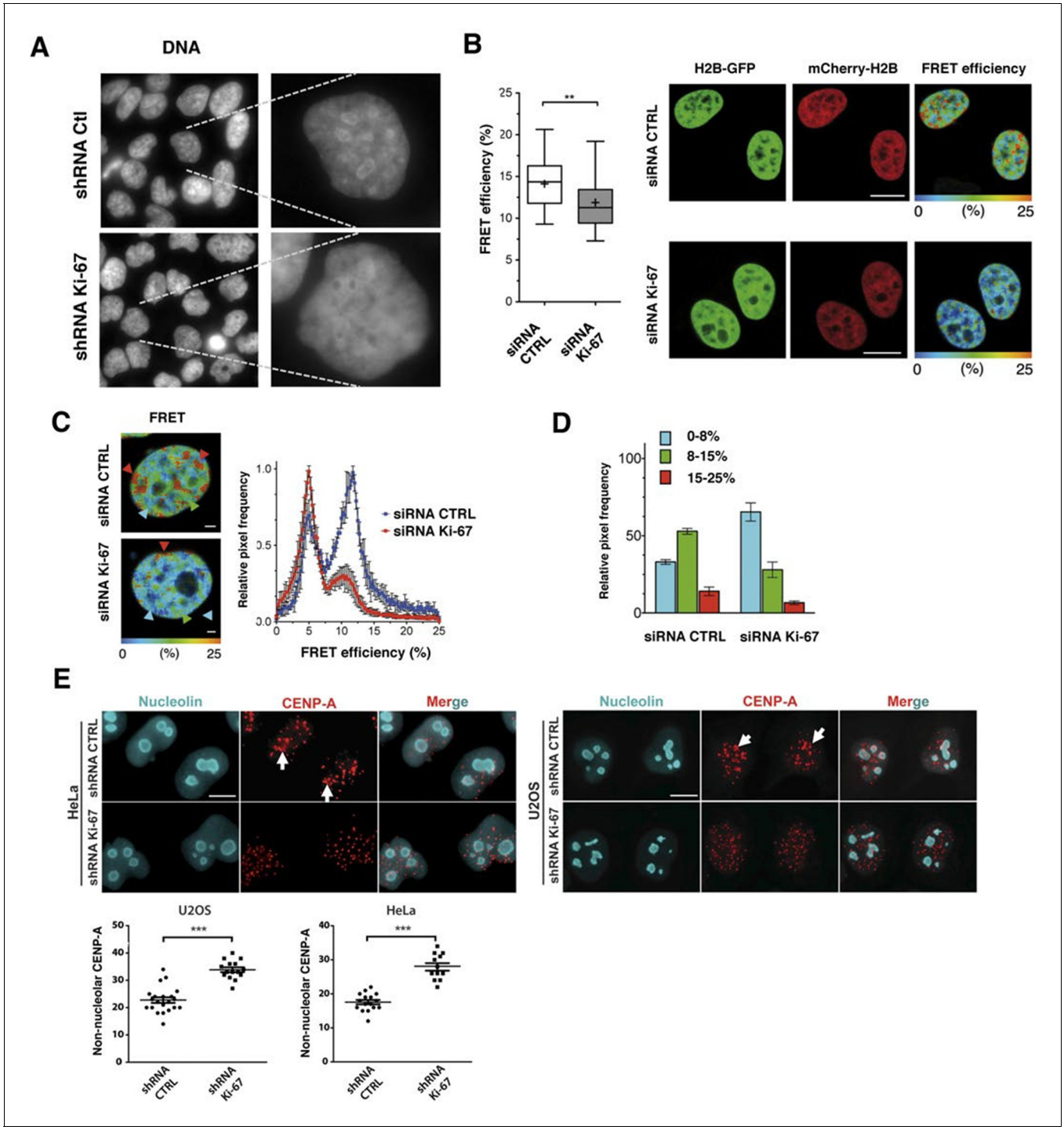

Figure 9. Ki-67 promotes heterochromatin interactions. (**A**) DAPI staining in control and stable Ki-67-knockdown U2OS cells. (**B**) HeLa cells stably expressing GFP-H2B and mCherry-H2B, depleted using Ki-67 or non-targeting (CTRL) siRNA. Left, FRET efficiency (cross shows mean value) ** Different, $p<0.01$. FRET efficiency and spatial distribution shown by a pseudocolour scale of FRET (%) values from 0 to 25%. Bars, 10 µm. (**C**) Left, representative HeLa$^{H2B-2FP}$ nuclei showing spatial distribution of FRET efficiency. Arrowheads show different chromatin compaction states (high FRET, red; intermediate, green; low, blue), Bars, 2 µm. Right, mean FRET distribution curves from siRNA control (blue curve, n=8) and siRNA Ki-67 (red curve, n=11) nuclei. (**D**) Relative fraction of the three FRET efficiency populations (blue (low), FRET efficiency $\leq$ 8%; green (medium), 8–15%; and red (high), 15–25%) in siRNA control and siRNA Ki-67 nuclei. Error bars indicate SD. (**E**) Immunofluorescence of CENP-A localisation in control and stable Ki-67 knockdown HeLa (left) and U2OS (right) cells. Nucleolar localisation (white arrows). Nucleolin was used as nucleolar marker. Bar, 10 µm. Below: quantification in different cells of numbers of CENP-A spots not associated with the nucleolus.

DOI: 10.7554/eLife.13722.037

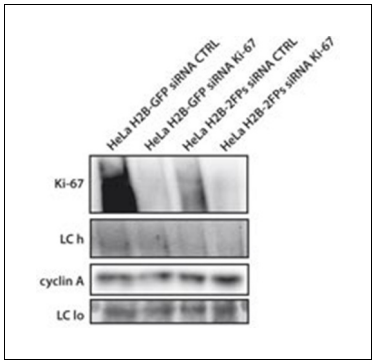

Figure 9—figure supplement 1. Knockdown of Ki-67 in H2B FRET cell line. Western blot analysis of the indicated proteins in asynchronously growing HeLa H2B FRET cells transiently transfected with control siRNA (Ctrl) or Ki-67 RNAi for 72 hr. LC, loading controls of the high (h) and low (lo) MW parts of the SDS-PAGE gel.

DOI: 10.7554/eLife.13722.038

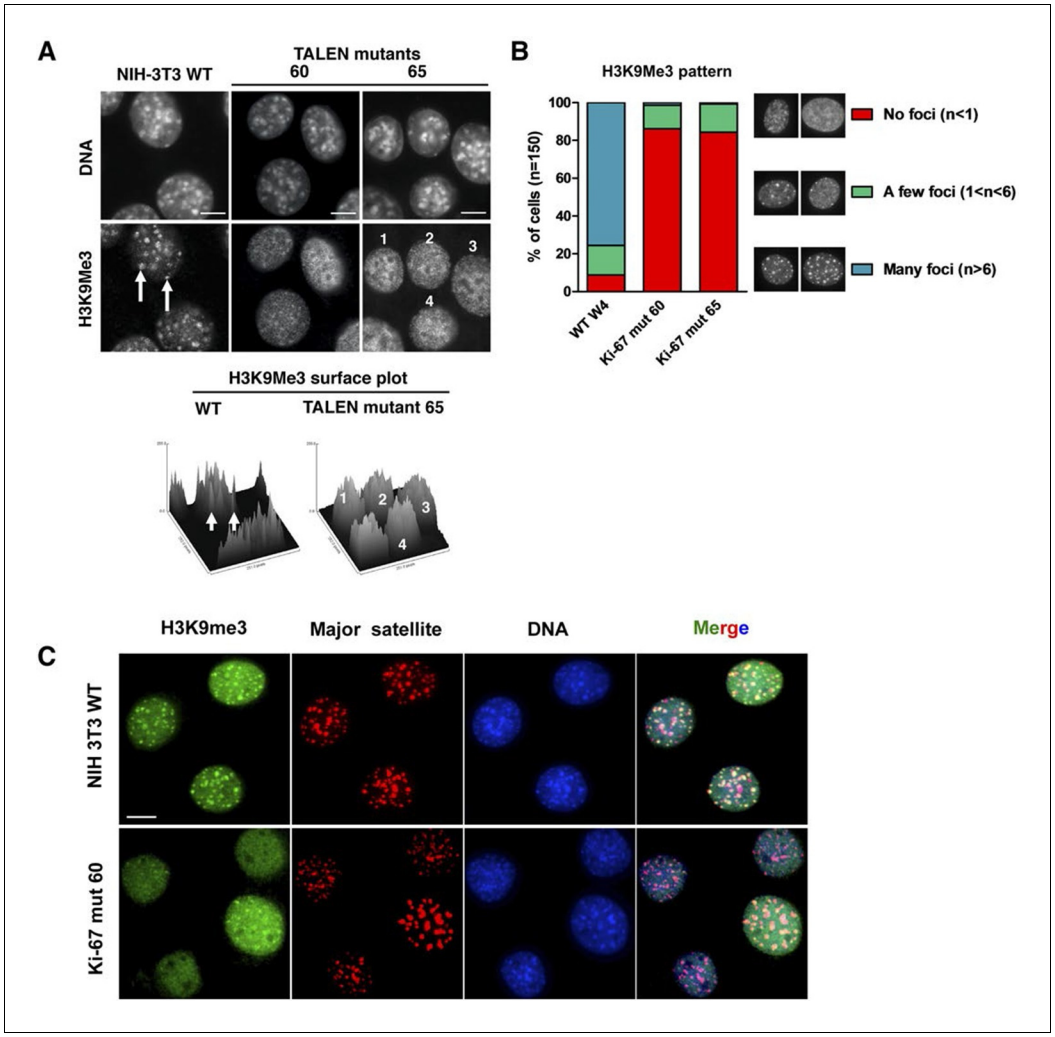

Figure 10. Ki-67 controls heterochromatin organisation. (**A**) Top, immunofluorescence analysis of H3K9me3 in mouse NIH-3T3 WT and *Mki67* TALEN mutant clones 60 and 65. Bars, 5 µm. Below: graphs showing quantification of pixel intensity scans for H3K9me3. (**B**) Quantification of H3K9Me3 patterns in WT and Ki-67 mutant clones. (**C**) Immunofluorescence of H3K9Me3, FISH of major satellite DNA and DAPI staining in WT W4 and Ki-67 mutant clone 60. Bar, 10 µm.

DOI: 10.7554/eLife.13722.039

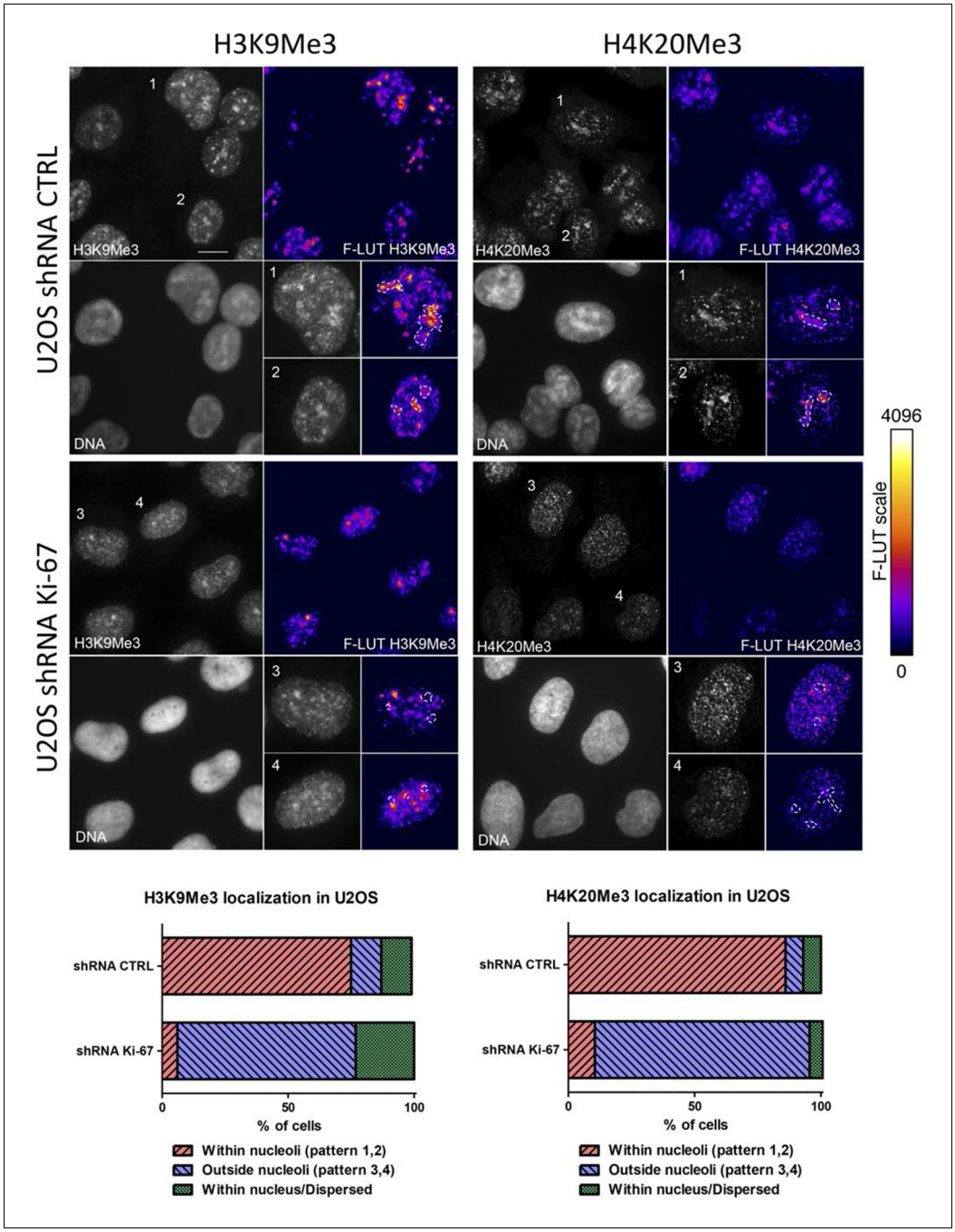

Figure 10—figure supplement 1. Heterochromatic histone mark localisation requires Ki-67. Immunofluorescence analysis of H3K9me3 (left) and H4K20me3 (right) localisation in stable control and Ki-67 knockdown U2OS cells. Right: Fire look up table (F-LUT) pseudocolouring of immunofluorescence staining intensity, generated using Fiji software (***Schindelin et al., 2012***). Dotted white lines denote nucleolus, while numbers 1–4 identify cells for insets as well as staining patterns within nucleolus (1,2) or outside the nucleolus (3,4). Histograms below show the percentage of cells counted showing each pattern. The 2D Fire-LUT surface plot was generated using Fiji software (1). Scale bar: 10 μm.

DOI: 10.7554/eLife.13722.040

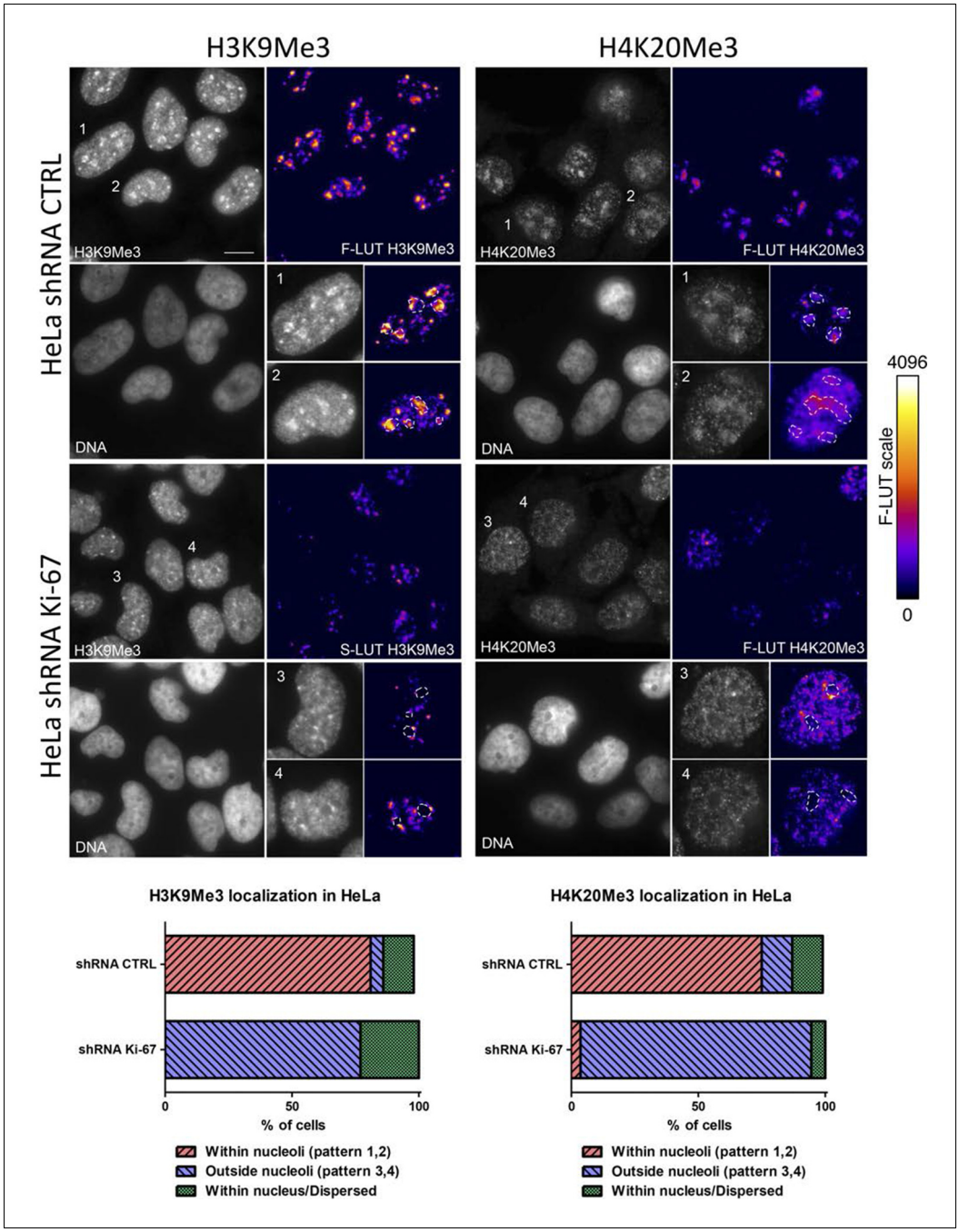

Figure 10—figure supplement 2. Heterochromatic histone mark localisation requires Ki-67. Immunofluorescence analysis of H3K9me3 (left) and H4K20me3 (right) localisation in stable control and Ki-67 knockdown HeLa cells. Right: Fire look up table (F-LUT) pseudocolouring of immunofluorescence staining intensity. Dotted white lines denote nucleolus, while numbers 1–4 identify cells for insets as well as staining patterns within nucleolus (1,2) or outside the nucleolus (3,4). Histograms below show the percentage of cells counted showing each pattern. Scale bar: 10 μm.

DOI: 10.7554/eLife.13722.041

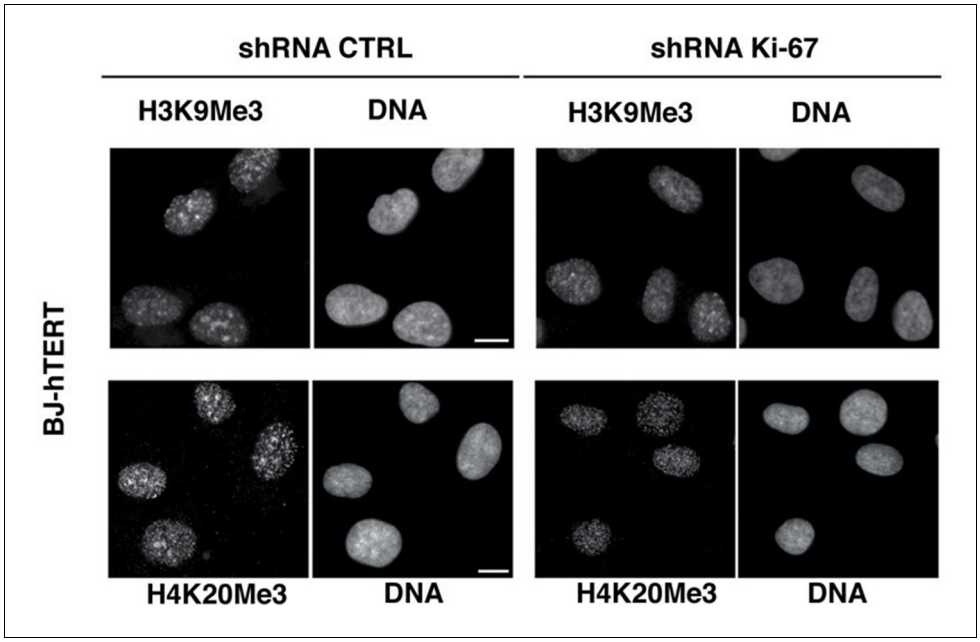

Figure 10—figure supplement 3. Heterochromatic histone mark localisation requires Ki-67. Immunofluorescence analysis of H3K9me3 and H4K20me3 localisation in stable control and Ki-67 knockdown hTERT immortalised human fibroblasts (HDF BJ hTERT) cells. Scale bars, 10 μm.
DOI: 10.7554/eLife.13722.042

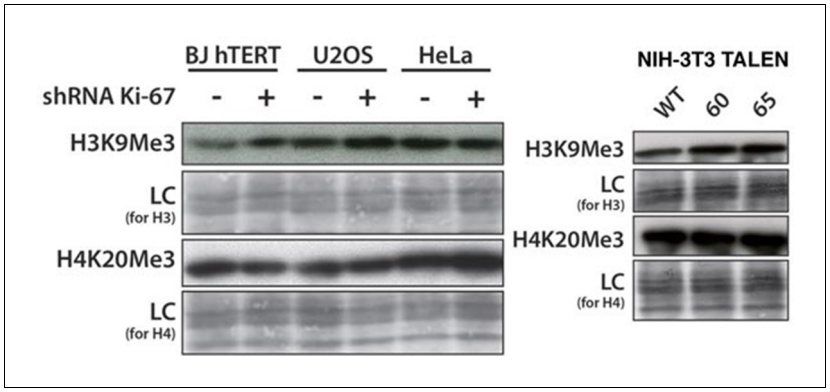

Figure 10—figure supplement 4. Overall heterochromatic histone mark levels do not change upon Ki-67 knockdown. Left: western blot of total H3K9me3 and H4K20me3 level in control and stable Ki-67 knockdown BJ-hTERT, U2OS and HeLa cells. LC, loading control. Right: western blot of total H3K9me3 and H4K20me3 level in NIH-3T3 WT clone W4 and Ki-67-negative TALEN clones 60, 65. LC, loading control

DOI: 10.7554/eLife.13722.043

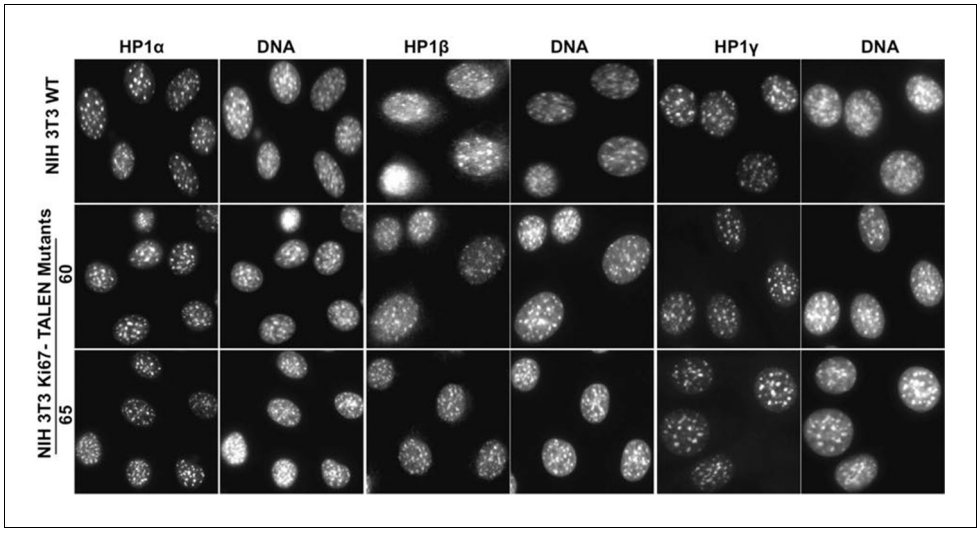

Figure 10—figure supplement 5. HP1 localises normally to chromocentres in Ki-67 mutant cells. Immunofluorescence analysis of localisation of HP1α, HP1β and HP1γ in WT and Ki-67-negative NIH-3T3 mutant clones 60 and 65, as compared with DAPI staining.

DOI: 10.7554/eLife.13722.044

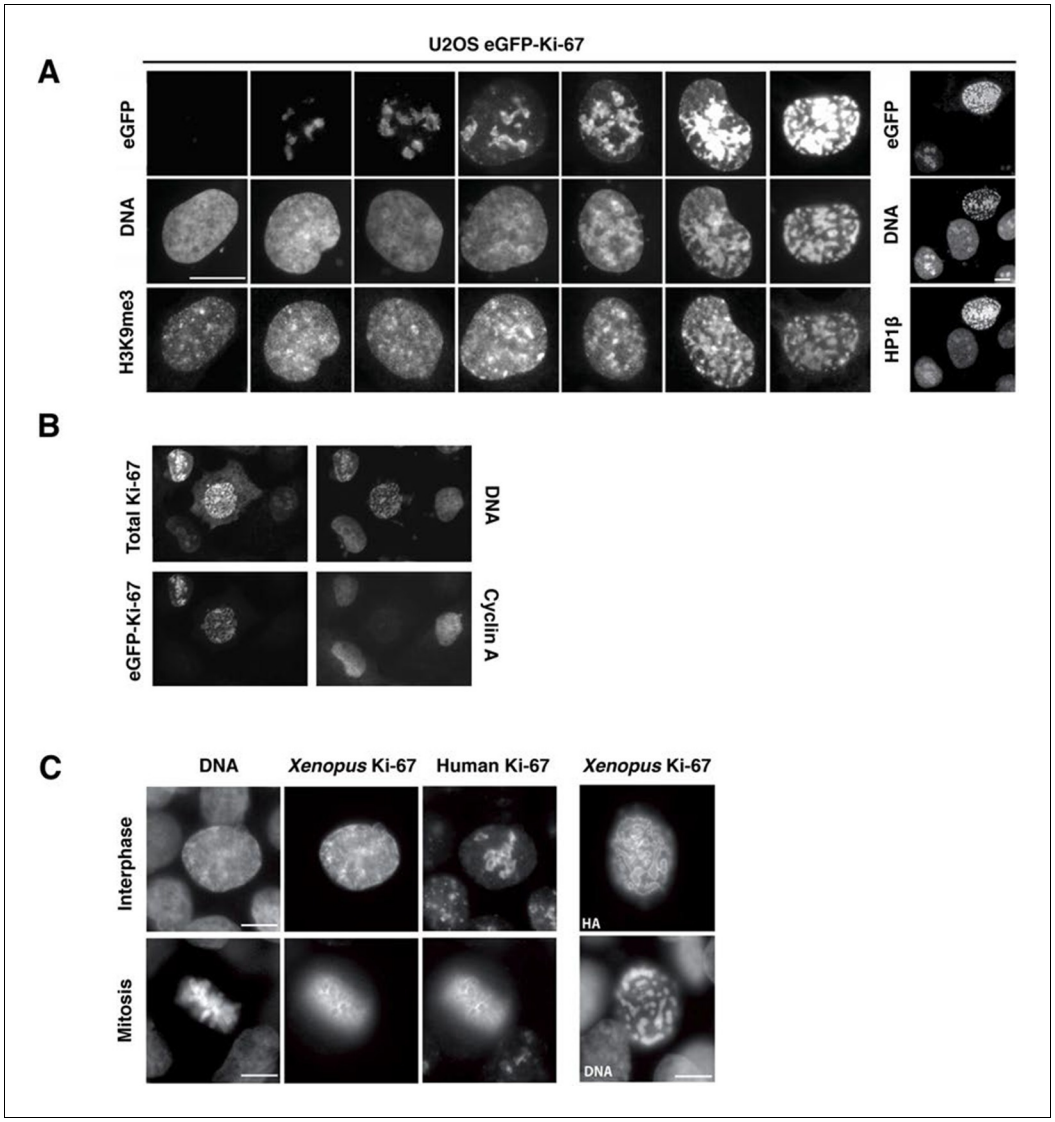

Figure 11. Overexpression of Ki-67 induces ectopic heterochromatin. (**A**) Overexpression of full length Ki-67 N-terminal fusion with eGFP in U2OS cells induces ectopic heterochromatin, as visualised by DAPI staining (middle) and immunofluorescence of H3K9Me3 (left) or HP1β (right). Eight representative cells that have different levels of Ki-67 expression, as determined by eGFP fluorescence intensity, are shown. Bar, 10 μm. (**B**) U2OS cells expressing high levels of exogenous eGFP-Ki-67 and showing ectopic chromatin condensation are negative for cyclin A staining by immunofluorescence. (**C**) Left: Immunofluorescence analysis of the localisation of endogenous human and ectopically expressed *Xenopus* Ki-67 in U2OS cells, showing colocalisation in metaphase at the perichromosomal region. Right: DNA condensation caused by high overexpression of *Xenopus* Ki-67 in U2OS cells. Bars, 10 μm.

DOI: 10.7554/eLife.13722.045

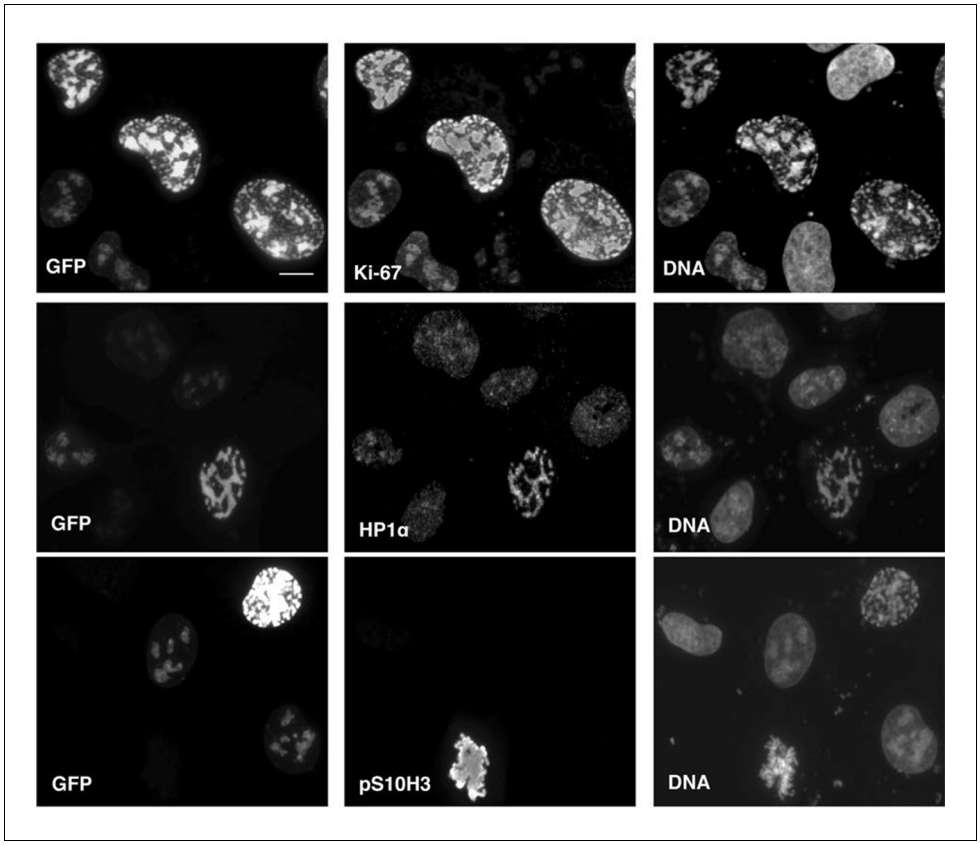

Figure 11—figure supplement 1. Overexpression of Ki-67 induces ectopic heterochromatin. Overexpression of full length Ki-67 N-terminal fusion with eGFP (GFP, left panels) in U2OS cells induces ectopic heterochromatin, as visualised by DAPI staining (DNA, right panels) or immunofluorescence of HP1α (centre, middle), whereas cells with lower Ki-67 expression levels have normal chromatin. Immunofluorescence of Ki-67 (top, middle) shows colocalisation of fusion protein with overall Ki-67 pattern. Immunofluorescence of phospho-histone H3S10 shows expected staining of mitotic metaphase (bottom, middle panel) but no staining in a cell with ectopic heterochromatin (top right cell, same panel) due to Ki-67 overexpression (GFP, bottom left panel). Bar, 10 μm
DOI: 10.7554/eLife.13722.046

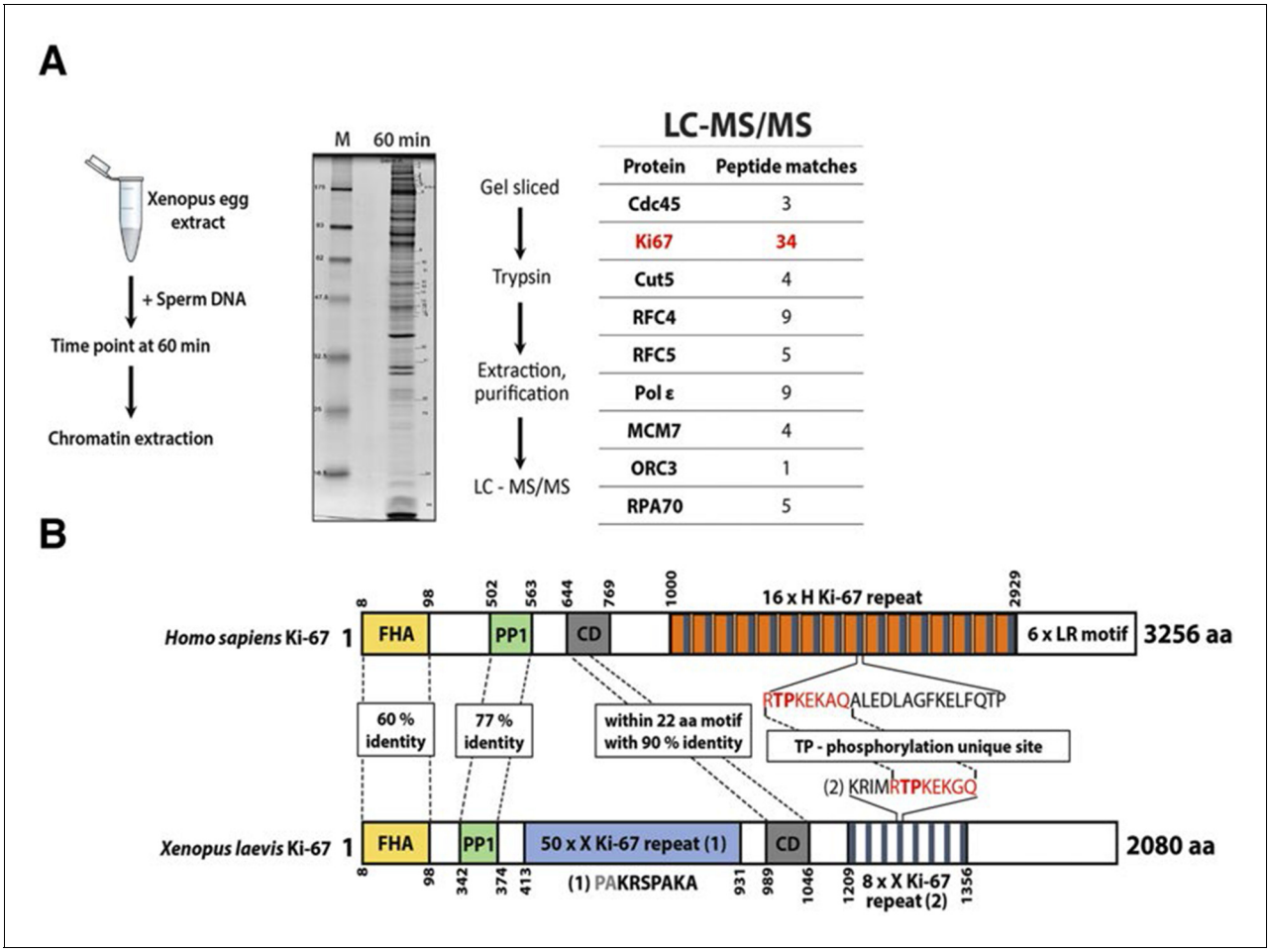

Figure 11—figure supplement 2. A Xenopus Ki-67 homologue (**A**) Chromatin proteomics in replicating *Xenopus* egg extracts. Scheme of the experiment and electrophoresis separation of sample processed and analysed by mass spectrometry. Table shows peptide matches. M, molecular weight marker. (**B**) Schematic comparison of *Xenopus* Ki-67 homologue with human Ki-67 (long form). Domains are indicated by boxes (FHA, forkhead-associated domain; PP1, PP1-binding domain; CD, conserved domain). Highly conserved regions are indicated by dotted line with percentage of identical amino acids. TP, threonine-proline phosphorylation site.

DOI: 10.7554/eLife.13722.047